Earth **Surface**
Dynamics
Discussions

Rarefied particle motions on hillslopes: 1. Theory

David Jon Furbish[1], Joshua J. Roering[2], Tyler H. Doane[1, 3], Danica L. Roth[2, 4], Sarah G. W. Williams[1], and Angel M. Abbott[1,†]

[1]Department of Earth and Environmental Sciences, Vanderbilt University, Nashville, Tennessee, USA
[2]Department of Earth Sciences, University of Oregon, Eugene, Oregon, USA
[3]Current: Department of Earth and Atmospheric Sciences, Indiana University, Bloomington, Indiana, USA
[4]Current: Department of Geology and Geological Engineering, Colorado School of Mines, Golden, Colorado, USA
[†]Deceased 10 August 2018

Correspondence: David Furbish (david.j.furbish@vanderbilt.edu)

Abstract. We describe the probabilistic physics of rarefied particle motions and deposition on rough hillslope surfaces. The particle energy balance involves gravitational heating with conversion of potential to kinetic energy, frictional cooling associated with particle-surface collisions, and an apparent heating associated with preferential deposition of low energy particles. Deposition probabilistically occurs with frictional cooling in relation to the distribution of particle energy states whose spatial

5   evolution is described by a Fokker-Planck equation. The Kirkby number Ki — defined as the ratio of gravitational heating to frictional cooling — sets the basic deposition behavior and the form of the probability distribution $f_r(r)$ of particle travel distances r, a generalized Pareto distribution. The shape and scale parameters of the distribution are well-defined mechanically. For isothermal conditions where frictional cooling matches gravitational heating plus the apparent heating due to deposition, the distribution $f_r(r)$ is exponential. With non-isothermal conditions and small Ki this distribution is bounded and represents

10   rapid thermal collapse. With increasing Ki the distribution $f_r(r)$ becomes heavy-tailed and represents net particle heating. It may possess a finite mean and finite variance, or the mean and variance may be undefined with sufficiently large Ki. The formulation provides key elements of the entrainment forms of the particle flux and the Exner equation, and it clarifies the mechanisms of particle-size sorting on large talus and scree slopes. Namely, with conversion of translational to rotational kinetic energy, large spinning particles are less likely to be stopped by collisional friction than are small or angular particles for

15   the same surface roughness.

1   Introduction

Sediment transport on steepland hillslopes involves a great range of scales of particle motions. These vary from relatively small motions that collectively produce the slow en masse motion of disturbance driven creep (Culling, 1963; Roering et al., 1999, 2002; Gabet, 2000; Anderson, 2002; Gabet et al., 2003; Furbish, 2003; Roering, 2004; Furbish et al., 2009b, 2018a) in concert

20   with athermal granular creep (Houssais and Jerolmack, 2017; BenDror and Goren, 2018; Ferdowsi et al., 2018; Deshpande et al., 2020) to the long-distance and relatively fast en masse motions of landsliding and the rarefied motions associated with rockfall and ravel (Kirkby and Statham, 1975; Statham, 1976; Dorren, 2003; Gabet, 2003; Roering and Gerber, 2005; Luckman, 2013; Tesson et al., 2020). Particularly in relation to long-distance motions, there is a growing interest in non-continuum

formulations of sediment transport on hillslopes that are aimed at accommodating nonlocal transport, where the particle flux at a hillslope position x depends on upslope conditions that influence the entrainment and motions of particles reaching x. These formulations include explicit particle-based descriptions (Tucker and Bradley, 2010) and probabilistic descriptions (Foufoula-Georgiou et al., 2009; Furbish and Haff, 2010; Furbish and Roering, 2013; Doane, 2018; Doane et al., 2018, 2019) of sediment

5 motions. Importantly, these descriptions do not hinge on satisfying a continuum-like behavior as assumed in most previous treatments of transport on hillslopes. Nonetheless, to date these particle-based and probabilistic descriptions of transport are mostly kinematic in form, lacking a formal mechanical underpinning.

Herein we focus on rarefied motions of particles which, once entrained, travel downslope over the land surface. This notably includes the dry ravel of particles down hillslopes following disturbances (Roering and Gerber, 2005; Doane, 2018; Doane et

10 al., 2019; Roth et al., 2020) or upon their release from obstacles (e.g., vegetation) following failure of the obstacles (Lamb et al., 2011, 2013; DiBiase and Lamb, 2013; DiBiase et al., 2017; Doane et al., 2018, 2019), and the motions of rock fall material over the surfaces of talus and scree slopes (Gerber and Scheidegger, 1974; Kirkby and Statham, 1975; Statham, 1976; Dorren 2003; Luckman, 2013) (Figure 1). By "rarefied motions" we are referring to the situation in which moving particles may frequently interact with the surface, but rarely interact with each other. Thus, rarefied particle motions are decidedly distinct from granular

15 flows. Indeed, processes such as rock fall and the subsequent motions of the rock material over talus or scree slopes represent the archetypal case of rarefied particle motions. Nonetheless, the ideas outlined below pertaining to the motions of individual particles may be entirely relevant to conditions that are not strictly rarefied, but where during the collective motions of many particles (e.g., during ravel) the effects of particle-surface interactions dominate over effects of particle-particle interactions in determining the behavior of the particles — akin to granular shear flows at high Knudsen number (Risso and Cordero, 2002;

20 Kumaran, 2005, 2006). We note that laboratory experiments (Kirkby and Statham, 1975; Gabet and Mendoza, 2012; Furbish et al., 2020a) and field-based experiments (DiBiase et al., 2017; Roth et al., 2020) designed to mimic particle motions and travel distances on hillslopes effectively focus on rarefied conditions.

The purpose of this paper is to provide a probabilistic description of the physics of rarefied particle motions and disentrainment. This involves threading together elements of statistical mechanics, concepts from granular gas theory, particle collision

25 mechanics, and probability distribution theory. To motivate the formalism we start in Section 2 with a probabilistic definition of the particle disentrainment rate and show its relation to the entrainment forms of the flux and the Exner equation, following previous presentations (Furbish and Haff, 2010; Furbish and Roering, 2013). This highlights how the disentrainment rate determines the probability distribution of travel distances, and thus connects descriptions of the flux and mass conservation with the physics of particle motions. In Section 3 we formulate disentrainment in terms of particle energetics, where the particles

30 are treated as a rarefied granular gas. Ensemble averaged motions are described in terms of a balance between gravitational heating and frictional cooling, wherein the latter leads to deposition. We neglect entrainment. (Our choice of terminology is based on that of granular physics as outlined in Appendix A.) The analysis in Section 4 illustrates the effects of collisional friction in determining the basic form of the distribution of travel distances, a generalized Pareto distribution. Depending on the balance between heating and cooling, this distribution transitions from a bounded form representing rapid thermal collapse

Figure 1. Image of talus slope at the base of cliffs of the Bandelier Tuff showing downslope sorting of particle sizes, with the largest particles preferentially accumulating near the base of the slope. The largest boulders in the foreground are about 1 m in diameter. As described in the text, we suspect that with conversion of translational to rotational kinetic energy, large spinning particles are less likely to be stopped by collisional friction than are small or angular particles for the same surface roughness, thus contributing to the sorting in this image. Image location is at the confluence of the Rito de los Frijoles river canyon with the Rio Grande River canyon on the eastern boundary of the Bandelier National Monument, New Mexico, USA.

to a heavy-tailed form representing net particle heating. In Section 5 we compare the formulation with previous mechanical descriptions of disentrainment, showing both similarities and dissimilarities with these descriptions.

We emphasize that this initial phase of our work on rarefied particle motions is aimed at clarifying how particle disentrainment works. With this in place we will be positioned to consider effects of rarefied transport over time scales spanning many transport events, including ensemble-averaged particle fluxes and changes in land-surface elevation as described by formulations of nonlocal transport. As a step in this effort we show in the second companion paper (Furbish et al., 2020a) that the theory in this first paper is entirely consistent with data from laboratory and field-based experiments involving measurements of particle travel distances on rough surfaces. These include data reported by Kirkby and Statham (1975), Gabet and Mendoza (2012), DiBiase et al. (2017) and Roth et al. (2020), and new travel distance data from laboratory experiments

supplemented with high-speed imaging and audio recordings that highlight effects of particle-surface collisions. Outstanding questions concern how particle size and shape in concert with surface roughness influence the extraction of particle energy and the likelihood of deposition. In the third companion paper (Furbish et al., 2020b) we show that the generalized Pareto distribution in this problem is a maximum entropy distribution (Jaynes, 1957a, 1957b) constrained by a fixed energetic "cost" — the total cumulative energy extracted by collisional friction per unit kinetic energy available during particle motions. That is, among all possible accessible microstates — the many different ways to arrange a great number of particles into distance states where each arrangement satisfies the same fixed total energetic cost — the generalized Pareto distribution represents the most probable arrangement. In the fourth companion paper (Furbish et al., 2020c) we step back and examine the philosophical underpinning of the statistical mechanics framework for describing sediment particle motions and transport.

2 Disentrainment rate

2.1 Continuous form

Following the presentations of Furbish and Haff (2010) and Furbish and Roering (2013), let $f_r(r;x)$ denote the probability density function of particle travel distances r whose motions begin at position x. By definition the cumulative distribution function is

$$F_r(r;x) = \int_0^r f_r(r';x)\, \mathrm{d}r',\tag{1}$$

where the prime denotes a variable of integration. In turn, the exceedance probability, also referred to as the survival function, is

$$R_r(r;x) = 1 - F_r(r;x) = \int_r^\infty f_r(r';x)\, \mathrm{d}r'.\tag{2}$$

With these definitions in place we now define the spatial disentrainment rate as

$$P_r(r;x) = \frac{f_r(r;x)}{1 - F_r(r;x)} = \frac{f_r(r;x)}{R_r(r;x)},\tag{3}$$

which is a conditional probability per unit distance. Namely, upon multiplying both sides of Eq. (3) by $\mathrm{d}r$, then $P_r(r;x)\mathrm{d}r = f_r(r;x)\mathrm{d}r/R_r(r;x)$ is interpreted as the probability that a particle will become disentrained within the small interval r to $r+\mathrm{d}r$, given that it "survived" travel to the distance r. The disentrainment rate $P_r(r;x)$ also may be interpreted as an inhomogeneous Poisson rate (Feller, 1949). Now, using the fact that $f_r(r;x) = -\mathrm{d}R_r(r;x)/\mathrm{d}r$, one may deduce from Eq. (3) that the probability density $f_r(r;x)$ is given by

$$f_r(r;x) = P_r(r;x)e^{-\int_0^r P_r(r';x)\,\mathrm{d}r'}.\tag{4}$$

Thus, according to Eq. (4), the disentrainment rate $P_r(r;x)$ completely determines the probability density $f_r(r;x)$ of travel distances r.

Assuming particle motions occur only in the positive x direction, the entrainment form of the volumetric particle flux is

$$q(x) = \int\limits_{-\infty}^{x} E_s(x') R_r(x-x';x') \, \mathrm{d}x', \tag{5}$$

where $E_s(x)$ denotes the volumetric entrainment rate at position x. In turn, letting $\zeta(x,t)$ denote the local land-surface elevation, the entrainment form of the Exner equation is (Tsujimoto, 1978; Nakagawa and Tsujiomoto, 1980)

$$5 \quad c_b \frac{\partial \zeta(x,t)}{\partial t} = -E_s(x) + \int\limits_{-\infty}^{x} E_s(x') f_r(x-x';x') \, \mathrm{d}x', \tag{6}$$

where $c_b = 1 - \phi_s$ is the particle volumetric concentration of the surface with porosity ϕ_s. These probabilistic formulations of the flux and the Exner equation have three lovely properties. They are mass conserving, they are nonlocal in form, and they are scale independent. They illustrate that the probability density $f_r(r;x)$ of particle travel distances r and its related survival function $R_r(r;x)$ form the centerpiece of describing mass conservation and the particle flux. In turn, the significance
10 of the disentrainment rate $P_r(r;x)$ becomes clear. This rate connects Eq. (5) and Eq. (6) to the physics of particle motions on a hillslope. That is, this rate, together with the entrainment rate $E_s(x)$, represent the elements in the formulation that can be elucidated by physics.

To date, previous formulations of the disentrainment rate $P_r(r;x)$ have envisioned a friction dominated behavior in which the land-surface slope $S(x) = |\partial \zeta(x)/\partial x|$ has a primary role (Furbish and Haff, 2010; Furbish and Roering, 2013; Doane, 2018;
15 Doane et al., 2018a; Section 5.3). The disentrainment rate is specified as a function of the land-surface slope at the position of entrainment, with the idea that the slope changes over a distance much larger than the average particle travel distance. That is, $P_r(r;x)$ is assumed to be a determined by the slope $S(x)$ at position x such that the distribution of travel distances of particles entrained at x is exponential with mean $\mu_r[S(x)]$. As the land-surface slope S varies with increasing downslope distance x, the mean $\mu_r[S(x)]$ changes. The disentrainment rate is qualitatively consistent with limiting cases, namely, it yields
20 a fixed small average travel distance at zero slope, and it approaches zero in the limit of a steep critical slope beyond which disentrainment does not occur. However, the mechanical elements of the disentrainment rate $P_r(r;)$ are otherwise not explicitly specified. We also note that Kirkby and Statham (1975) first pointed out the relation between the distribution of travel distances and the disentrainment rate function. These authors defined *a posteriori* the disentrainment rate from an assumed exponential distribution of travel distances whose mean value is expressed in terms of a Coulomb-like description of particle friction
25 (Section 5.1).

2.2 Discrete form

It is valuable to recast the ideas of disentrainment above in discrete form. The motivation is this. Instead of trying to formulate a continuous disentrainment rate function that is generally applicable to the entirety of a hillslope, we instead break it into discrete spatial intervals, where certain physics may be more or less important in some intervals than in others. This gets us
30 closer to the physical ingredients of disentrainment that are occurring at different locations on a hillslope, where the mechanical

behavior at a location transitions to another behavior in the downslope direction. We may then combine the intervals together as a whole.

Let $k = 1, 2, 3, ...$ denote a set of discrete intervals of length dr. Let p denote the probability that a particle is disentrained within the first interval ($k = 1$). If N denotes a great number of particles, then the number of particles $n(1)$ disentrained within

5   the first interval is $n(1) = Np$. Because $q = 1 - p$ is the probability that a particle is not disentrained within the first interval, then the number of particles moving beyond the first interval is $Nq = N(1 - p)$. That is, this is the number of particles that "survived" without being disentrained within the first interval. In turn, of the number of particles that survived, the number that is disentrained within the second interval is $n(2) = N(1 - p)p$. More generally, $n(k) = N(1 - p)^{k-1}p$. Dividing this by N then gives the probability mass function

10   $$f_k(k) = (1 - p)^{k-1}p = q^{k-1}p,$$ (7)

which defines the well-known geometric distribution with mean $\mu_k = 1/p$. Note that the probability p is taken here as being fixed. That is, in this formulation, the probability that a particle survives the kth interval is $(1 - p)^{k-1}$, so the disentrainment probability is constant, namely, $P_k(k) = p$.

The geometric distribution, Eq. (7), is the discrete counterpart of the exponential distribution. Here we relate the two. The

15   cumulative distribution function of Eq. (7) is $F_k(k) = 1 - (1 - p)^k$. We may thus write $F_r(r = kdr) = F_k(k) = 1 - q^k$. The quantity q^k is a memoryless geometric series, and because $q \leq 1$ we may write $q = e^{-dr/\mu_r}$, where μ_r is a characteristic distance. In turn, then, $F_r(r) = 1 - (e^{-dr/\mu_r})^k = 1 - e^{-r/\mu_r}$. Finally, $f_r(r) = dF_r(r)/dr = (1/\mu_r)e^{-r/\mu_r}$, where it becomes clear that μ_r is the mean of the exponential distribution, analogous to μ_k for the discrete counterpart. Also note that the disentrainment rate $P_r(r) = 1/\mu_r$ is fixed. Below we show that the exponential and geometrical distributions represent isothermal

20   conditions, where gravitational heating of particles is balanced by frictional cooling.

In contrast, suppose that the probability of disentrainment p varies from one interval k to another. Here we generalize the ideas above. Let p_k denote the probability that a particle, having not been disentrained before the kth interval, then becomes disentrained within this interval. Similar to the formulation above, the number of particles $n(1)$ within the first interval is $n(1) = Np_1$ and the number moving beyond the first interval is $N(1 - p_1)$. In turn the number of particles disentrained within

25   the second interval is $n(2) = N(1 - p_1)p_2$, the number disentrained within the third interval is $N(1 - p_1)(1 - p_2)p_3$, and so on. In general, $n(k) = N(1 - p_1)(1 - p_2)(1 - p_3)...(1 - p_{k-1})p_k$. Dividing this expression by N then gives

$$f_k(k) = p_k \prod_{i=1}^{k-1} (1 - p_i).$$ (8)

Note that if $p_k = p$ is fixed, then Eq. (8) reduces to Eq. (7).

This generalization has a lovely property. Namely, by definition it conserves probability, and it therefore is mass conserving.

30   That is, the sum of $f_k(k)$ over all possible k is equal to unity, regardless of how p_k might vary with k. As alluded to above, the physics of each p_k may be treated differently if desired. Moreover, like its continuous counterpart presented above, this discrete formulation of mass conservation is nonlocal and scale independent.

We now set these results aside. Our next objective is to illustrate the mechanical elements of disentrainment, which we then use to elaborate the continuous and discrete cases described above.

3 Mechanical interpretation of disentrainment

3.1 Conservation of mass

Consider a rough, inclined surface with uniform slope angle θ (Figure 2). At this juncture we simplify the notation and consider
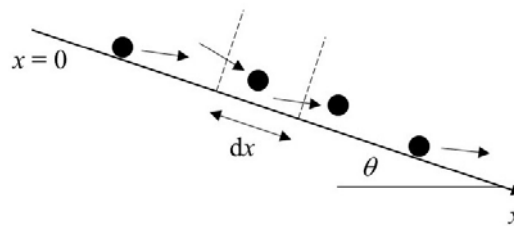

Figure 2. Definition diagram of surface inclined at angle θ and control volume with edge length $\mathrm{d}x$ through which particles move.

5

the motions of particles entrained at a single position $x = 0$. Now the particle travel distance $r \to x$ and the probability density function $f_r(r; x) \to f_x(x)$. Consider a control volume with edge length $\mathrm{d}x$ parallel to the mean particle motion. Over a period of time a great number of particles enters the left face of the control volume. Some of these particles move entirely through the volume, exiting its right face, and some come to rest within the control volume. Many, but not necessarily all, of the particles

10 interact with the surface one or more times in moving through the volume or in being disentrained within it.

We now imagine collecting this great number of particles and treat them as a cohort, independent of time (Appendix B). That is, let $N(x)$ denote the number of particles that enter the control volume, and let $N(x + \mathrm{d}x)$ denote the number that leaves the volume. We may imagine for the purpose of visualizing the problem that the $N(x)$ particles enter the control volume at the same time, but this actually is not essential. Similarly, we may imagine that the $N(x + \mathrm{d}x)$ particles exit the control volume at

15 approximately the same time, but again, this reference to time only is a means to envision particle motions (Appendix B). The number of particles disentrained within the control volume then is $\mathrm{d}N = N(x + \mathrm{d}x) - N(x)$.

If $N(0)$ denotes the great number of particles whose motions started at position $x = 0$, then the exceedance probability $R_x(x)$ (analogous to $R_r(r; x)$ above) is $R_x(x) = N(x)/N(0)$. Then $\mathrm{d}N = -N(0)f_x(x)\mathrm{d}x$ and the spatial disentrainment rate $P_x(x)$ (analogous to $P_r(r)$ above) is

20
$$P_x(x) = -\frac{1}{N(x)}\frac{\mathrm{d}N(x)}{\mathrm{d}x}. \tag{9}$$

Our objective is to determine the derivative $\mathrm{d}N(x)/\mathrm{d}x$ in relation to particle energy, as this derivative represents disentrainment. Here we summarize the essence of this problem before turning to a description of conservation of energy.

Let $E_p = (m/2)u^2$ denote the translational kinetic energy of a particle with mass m and downslope velocity u. Here we are assuming that the total translational energy is dominated by downslope motion. Let $f_{E_p}(E_p, x)$ denote the probability density function of particle energies E_p as these vary with position x. For a great number N of particles the number density is $n_{E_p}(E_p, x) = N f_{E_p}(E_p, x)$. Let $p(E_p, x)$ denote the probability that a particle at energy state E_p will become disentrained within the small interval x to $x + \mathrm{d}x$. Because $N f_{E_p}(E_p, x)\mathrm{d}E_p$ is the number of particles within the small interval E_p to $E_p + \mathrm{d}E_p$, then $N p(E_p, x) f_{E_p}(E_p, x)\mathrm{d}E_p$ is the number of particles in this energy interval that becomes disentrained. The total number of particles that becomes disentrained within the interval x to $x + \mathrm{d}x$ is then

$$\mathrm{d}N(x) = -N(x) \int_0^\infty p(E_p, x) f_{E_p}(E_p, x)\mathrm{d}E_p. \tag{10}$$

Letting angle brackets denote an ensemble average, then according to the Law of the Unconscious Statistician, Eq. (10) is simply $\mathrm{d}N(x) = -N(x)\langle p(E_p, x)\rangle$. Below we introduce the expected number of particle-surface collisions per unit distance $n_x = 1/\lambda$, where λ is the expected travel distance between successive collisions. We then show that $\mathrm{d}N(x)/\mathrm{d}x = -N(x)n_x\langle p(E_p, x)\rangle$. Thus, the essence of the problem is to determine the averaged probability $\langle p(E_p, x)\rangle$ as this depends on particle energy E_p. This in turn requires specifying the particle energy as this varies with position x.

3.2 Particle energy

We start our formulation with a general statement concerning conservation of the kinetic energy of a system of particles. Because of its familiarity in relation to studies of granular gas systems, we initially consider changes with respect to time, then return to changes with respect to space as in the preceding section. Namely, let E_p denote the kinetic energy of a particle, and let $\langle E_p \rangle$ denote the expected energy state, where angle brackets represent an ensemble average over a great number N of moving particles. The total energy of the system is $E = N\langle E_p \rangle$. Neglecting transport of energy, the rate of change in the total energy of the system with respect to time is then

$$\frac{\mathrm{d}E}{\mathrm{d}t} = N\frac{\mathrm{d}\langle E_p \rangle}{\mathrm{d}t} + \langle E_p \rangle\frac{\mathrm{d}N}{\mathrm{d}t}. \tag{11}$$

The first term on the right side of Eq. (11) represents the rate of change in the average energy state of N moving particles, and thus describes either a net heating ($\mathrm{d}\langle E_p \rangle/\mathrm{d}t > 0$) or cooling ($\mathrm{d}\langle E_p \rangle/\mathrm{d}t < 0$) of the system, depending on the relative contribution of the sources of each. The second term on the right side represents the rate of change in the number of moving particles with average energy state $\langle E_p \rangle$, and thus describes the rate of change in the total energy due to either the addition or loss of moving particles. For a closed system, this represents either a net sublimation ($\mathrm{d}N/\mathrm{d}t > 0$) or net deposition ($\mathrm{d}N/\mathrm{d}t < 0$) of particles, depending on the relative contribution of each.

The first term on the right side of Eq. (11) has been studied extensively for granular gas systems, specifically in relation to the "homogeneous cooling state" of a closed system as described by Haff's cooling law (Haff, 1983; Brilliantov and Pöschel, 2004; Dominguez and Zenit, 2007; Volfson et al., 2007; Brilliantov et al., 2018; Yu et al., 2020). In what follows, we start with similar concepts of particle energy; but the formulation is designed to be independent of time and focused on changes in energy and particle disentrainment over space.

Reconsider a control volume with edge length $\mathrm{d}x$ parallel to the mean motion of particles over a rough, inclined surface (Figure 2). Analogous to Eq. (11) we write

$$\frac{\mathrm{d}E}{\mathrm{d}x} = N\frac{\mathrm{d}\langle E_p \rangle}{\mathrm{d}x} + \langle E_p \rangle \frac{\mathrm{d}N}{\mathrm{d}x}\,, \tag{12}$$

where now the angle brackets formally denote a Gibbs ensemble average over a cohort of particles (Appendix B). As described
5 below, the first term on the right side of Eq. (12) represents the spatial rate of change in energy due to the sum of gravitational heating and frictional cooling. The second term on the right side represents the rate of change in energy due to deposition, that is, disentrainment. In this problem, we assume that sublimation (entrainment) does not occur over $x > 0$. Eq. (12) provides a basic starting point. However, it is not particularly useful in this form. If in fact the probability of deposition varies with energy state, then in general the derivative $\mathrm{d}N/\mathrm{d}x$ contributes to the derivative $\mathrm{d}\langle E_p \rangle/\mathrm{d}x$, as removal of energy by deposition
10 affects the average energy of the remaining particles. We note that Brilliantov et al. (2018) demonstrate an analogous effect, as described below, associated with aggregation of particles in a granular gas. We therefore must be careful in formulating a statement of conservation of particle energy, as deposition preferentially involves particles at low energy states.

Here is a sidebar concerning our focus on conservation of particle energy versus momentum. Particle motions down a rough hillslope surface involve numerous details that control momentum exchanges during particle-surface interactions. As a
15 scalar quantity, energy forces us to blur our eyes appropriately, focusing on the essence of these complex interactions rather than attempting to describe details of momentum exchanges that ultimately cannot be constrained given the stochastic nature of the phenomenon. As an example, below we introduce the random variable β_x to represent the proportion of downslope kinetic energy extracted during a particle-surface collision. This quantity blurs over many details (e.g., differences between collisions during rolling, tumbling and bouncing motions, rotational versus translational motion, and the roles of normal and
20 tangential coefficients of restitution), yet β_x is entirely meaningful when treated as a random variable. (We provide a description (Appendix E) of how the energy-centric quantity β_x is related to momentum exchanges during collisions, and in the companion paper we illustrate the elements of β_x using high-speed imaging.) In contrast, when describing the collisional behavior of an ideal granular gas, one can at lowest order appeal to a single coefficient of restitution because of the relative simplicity of the particles and their collisions (e.g., Haff, 1983; Jenkins and Savage, 1983). This simplicity is not possible here. The focus on
25 energy thus offers tractable and defensible simplicity amidst the messiness of natural hillslopes.

3.3 Conservation of energy

3.3.1 Total energy

Focusing just on slope parallel motions, let $E_p = (m/2)u^2$ denote the translational kinetic energy of a particle with mass m and downslope velocity u. Then let $f_{E_p}(E_p, x)$ denote the probability density function of particle energies E_p as these vary
30 with downslope position x (Appendix B). For a great number N of particles the number density is $n_{E_p}(E_p, x) = Nf_{E_p}(E_p, x)$.

The average particle energy is

$$\langle E_p \rangle = \int_0^\infty E_p f_{E_p}(E_p, x)\, \mathrm{d}E_p$$

$$= \frac{1}{N} \int_0^\infty E_p n_{E_p}(E_p, x)\, \mathrm{d}E_p\,. \tag{13}$$

5   The total energy $E(x) = N\langle E_p \rangle$, so

$$E(x) = \int_0^\infty E_p n_{E_p}(E_p, x)\, \mathrm{d}E_p\,. \tag{14}$$

We now take the derivative of Eq. (14) with respect to x using Leibniz's rule to give

$$\frac{\mathrm{d}E(x)}{\mathrm{d}x} = \int_0^\infty E_p \frac{\partial n_{E_p}(E_p, x)}{\partial x}\, \mathrm{d}E_p\,. \tag{15}$$

The derivative within the integral of Eq. (15) satisfies a Fokker-Planck equation (see next section and Appendix C), the solution

10   of which represents the evolution of the distribution $n_{E_p}(E_p, x)$ of particle energy states E_p with distance x. In particular this
derivative has three parts. The first part, denoted below by $K_h(E_p, x)$, is associated with a change in the density $n_{E_p}(E_p, x)$
due to gravitational heating. The second part, $K_c(E_p, x)$, is associated with a change in this density due to frictional cooling. The
third part, $K_d(E_p, x)$, is associated with a loss of energy due to deposition (which does not involve the analogue of release
of latent heat; but see below). We thus write

15   $$\frac{\partial n_{E_p}(E_p, x)}{\partial x} = K_h(E_p, x) + K_c(E_p, x) + K_d(E_p, x)\,, \tag{16}$$

and then rewrite Eq. (15) as

$$\frac{\mathrm{d}E(x)}{\mathrm{d}x} = \int_0^\infty E_p K_h(E_p, x)\, \mathrm{d}E_p$$

$$+ \int_0^\infty E_p K_c(E_p, x)\, \mathrm{d}E_p$$

20

$$+ \int_0^\infty E_p K_d(E_p, x)\, \mathrm{d}E_p\,. \tag{17}$$

The next task consists of showing the correspondence of $K_h(E_p, x)$, $K_c(E_p, x)$ and $K_d(E_p, x)$ to terms in the Fokker-Planck
equation, then describing the physical elements of these terms. This is followed by evaluating each of the integral quantities in
Eq. (17). There are a lot of moving parts in this formulation, so bear with us.

3.3.2 Fokker-Planck-like equation

The density $n_{E_p}(E_p, x)$ within Eq. (15) and Eq. (16) satisfies a Fokker-Planck equation (Appendix C), which describes the evolution of this density with increasing distance x. Namely,

$$\frac{\partial n_{E_p}(E_p, x)}{\partial x} = -\frac{\partial}{\partial E_p}[k_{1h}(E_p, x)n_{E_p}(E_p, x)]$$

5

$$-\frac{\partial}{\partial E_p}[k_{1c}(E_p, x)n_{E_p}(E_p, x)]$$

$$+\frac{1}{2}\frac{\partial^2}{\partial E_p^2}[k_{2c}(E_p, x)n_{E_p}(E_p, x)]$$

10

$$-K_d(E_p, x). \tag{18}$$

The first term on the right side of Eq. (18) represents advective gravitational heating, where $k_{1h}(E_p, x)$ is a drift speed, the average spatial rate of change in particle energy over the energy domain due to heating. The second term on the right side represents advective frictional cooling, where $k_{1c}(E_p, x)$ is a drift speed, the average spatial rate of change in particle energy due to cooling. The third term represents diffusive frictional cooling, where $k_{2c}(E_p, x)$ is a diffusion coefficient. The last

15   term represents a loss of energy due to deposition, where for now we have retained the notation from above. Explicitly, for $K_h(E_p, x)$ and $K_c(E_p, x)$ we now have

$$K_h(E_p, x) = -\frac{\partial}{\partial E_p}[k_{1h}(E_p, x)n_{E_p}(E_p, x)] \tag{19}$$

and

$$K_c(E_p, x) = -\frac{\partial}{\partial E_p}[k_{1c}(E_p, x)n_{E_p}(E_p, x)]$$

20

$$+\frac{1}{2}\frac{\partial^2}{\partial E_p^2}[k_{2c}(E_p, x)n_{E_p}(E_p, x)]. \tag{20}$$

In the next section we step through gravitational heating, frictional cooling and deposition, in each case unfolding the mechanical elements of $k_{1h}(E_p, x)$, $k_{1c}(E_p, x)$, $k_{2c}(E_p, x)$ and $K_d(E_p, x)$.

Here is a didactic sidebar if the formulation above seems counterintuitive. Notice that Eq. (18) effectively represents an

25   advection-diffusion equation with two advective terms, a diffusive term and a sink term. Normally we think of an advection-diffusion equation as involving space and time, that is, where the rate at which a quantity changes with respect to time at a given position is equal to the sum of an advective term and a diffusive term involving derivatives of the quantity with respect to space. Indeed, imagine replacing E_p with x, and x with t, in Eq. (18). The result looks like a familiar advection-diffusion equation with a sink term (albeit involving two advective terms rather than one). The basic idea of Eq. (18) is the same. It just

describes the rate of change in n_{E_p} with respect to position x (rather than time t) in relation to advection and diffusion of n_{E_p} occurring over the energy coordinate E_p (rather than x). A consideration of the rate of change with respect to position x as in Eq. (18) is perhaps unusual, but the idea of advection and diffusion of a quantity occurring over a domain other than a spatial coordinate (e.g., a velocity coordinate) is common in statistical physics, of which examples pertaining to sediment motions

5   include those presented in Furbish et al. (2012, 2018a, 2018b).

3.3.3   Gravitational heating

We start by noting that the rate at which the potential energy of a particle is converted to kinetic energy per unit distance x is $mg\sin\theta$. To be clear, between collisions a particle that is not in contact with the inclined surface beneath it accelerates vertically at a rate of $-g$, independently of the orientation of the surface. The factor $\sin\theta$ therefore is a geometrical constraint

10   on the magnitude of the potential energy that is accessible for net heating when viewed with respect to x. This means that (Appendix C)

$$k_{1h}(E_p,x) \rightarrow k_{1h} = mg\sin\theta\,, \tag{21}$$

so that Eq. (19) becomes

$$K_h(E_p,x) = -mg\sin\theta \frac{\partial n_{E_p}(E_p,x)}{\partial E_p}\,. \tag{22}$$

15   We now write the first integral in Eq. (17) as

$$-mg\sin\theta \int_0^\infty E_p \frac{\partial n_{E_p}(E_p,x)}{\partial E_p}\,\mathrm{d}E_p\,. \tag{23}$$

Because $\partial(E_p n_{E_p})/\partial E_p = E_p \partial n_{E_p}/\partial E_p + n_{E_p}$, Eq. (23) may be written as

$$mg\sin\theta \int_0^\infty n_{E_p}(E_p,x)\,\mathrm{d}E_p$$

20   $$-mg\sin\theta \int_0^\infty \frac{\partial}{\partial E_p}[E_p n_{E_p}(E_p,x)]\,\mathrm{d}E_p\,. \tag{24}$$

Assuming $n_{E_p}(\infty,x) \rightarrow 0$, the second integral in Eq. (24) vanishes and the first integral in Eq. (17) becomes

$$\int_0^\infty E_p K_h(E_p,x)\,\mathrm{d}E_p = Nmg\sin\theta\,. \tag{25}$$

Note that the form of the density $n_{E_p}(E_p,x)$ is immaterial in this formulation.

If for illustration we assume that no cooling or deposition occurs, then $\mathrm{d}E(x)/\mathrm{d}x = Nmg\sin\theta$. The solution of this

25   is $E(x) = E(0) + Nmg\sin\theta x$, where $E(0)$ denotes the starting energy at $x = 0$. That is, the total energy $E(x)$ increases

linearly with downslope distance x. Moreover, for reference below, no particle can be heated to an energy greater than $E_p(0) + mg\sin\theta x$, representing a complete conversion of gravitational to kinetic energy without any loss due to particle-surface collisions. This ensures that the density $n_{E_p}(E_p, x)$ is bounded with finite mean and variance, a point that becomes useful below.

3.3.4 Frictional cooling

We start by assuming that a change in the downslope energy of a particle associated with a collision is $\Delta E_p = -\beta_x E_p$, so that $\beta_x = -\Delta E_p/E_p$ is the proportion of energy extracted by the collision (Appendix E). By definition β_x is a random variable. (Note that the negative sign above is by convention. As a random variable we are assuming that $0 \le \beta_x \le 1$. The sign associated with β_x will be clear from the context in the developments below.) The change ΔE_p includes frictional loss, any conversion of translational to rotational energy, and any apparent change when downslope incident motion is reflected to transverse motion during a glancing particle-surface collision. Note that ΔE_p generally is a negative quantity. But strictly speaking it could be positive, albeit with low probability, if transverse incident motion is reflected to downslope motion during a collision. Because E_p and β_x are random variables, ΔE_p is a random variable. As a point of reference, in granular gas theory where the total translational energy is considered rather than just the energy associated with one coordinate direction, the proportion $\beta_x = 1 - \epsilon^2$ where ϵ is the normal coefficient of restitution (Haff, 1983). Moreover, ϵ is treated as a fixed deterministic quantity rather than a random variable. Here, in contrast, collision mechanics theory suggests that the constitution of β_x is far more complicated in relation to normal, tangential and rotational impulses during particle-surface collisions (Appendix E).

Let $q = E_p(x + \mathrm{d}x) - E_p(x)$ denote a change in the energy of a particle over the small distance $\mathrm{d}x$. Then as described in Appendix C, the drift speed $k_{1c}(E_p, x) = \mathrm{d}\bar{q}/\mathrm{d}x \approx n_x \overline{\beta_x} E_p$ and the diffusion coefficient $k_{2c} = \mathrm{d}\overline{q^2}/\mathrm{d}x \approx n_x \overline{\beta_x^2} E_p^2$, where the overline denotes an average over particles at the energy state E_p (rather than an ensemble average), and $n_x = 1/\lambda$ denotes the expected number of particle-surface collisions per unit distance where λ is the expected travel distance between collisions. Scaling (Appendix D) shows that

$$n_x = \frac{1}{\lambda} \approx \frac{mg\cos\theta}{4E_p\tan\phi}, \tag{26}$$

where ϕ is the expected reflection angle of a particle with energy E_p following a surface collision. We now assume that

$$k_{1c}(E_p, x) \sim n_x \overline{\beta_x} E_p \approx \frac{mg\overline{\beta_x}\cos\theta}{4\tan\phi}, \tag{27}$$

and that

$$k_{2c}(E_p, x) \sim n_x \overline{\beta_x^2} E_p^2 \approx \frac{mg\overline{\beta_x^2} E_p \cos\theta}{4\tan\phi}. \tag{28}$$

Now Eq. (20) becomes

$$K_c(E_p, x) = \frac{mg\cos\theta}{4\tan\phi} \frac{\partial}{\partial E_p}[\overline{\beta_x} n_{E_p}(E_p, x)]$$

$$+ \frac{mg\cos\theta}{8\tan\phi} \frac{\partial^2}{\partial E_p^2}[\overline{\beta_x^2}E_p n_{E_p}(E_p,x)]. \tag{29}$$

We now use these results to write the second integral in Eq. (17) as

$$\frac{mg\cos\theta}{4\tan\phi} \int\limits_0^\infty E_p \frac{\partial}{\partial E_p}[\overline{\beta_x}n_{E_p}(E_p,x)]\,\mathrm{d}E_p$$

5

$$+ \frac{mg\cos\theta}{8\tan\phi} \int\limits_0^\infty E_p \frac{\partial^2}{\partial E_p^2}[\overline{\beta_x^2}E_p n_{E_p}(E_p,x)]\,\mathrm{d}E_p. \tag{30}$$

Upon applying the product rule to the derivative $\partial(E_p\overline{\beta_x}n_{E_p})/\partial E_p$, the first integral in Eq. (30) may be written as

$$\int\limits_0^\infty \overline{\beta_x}n_{E_p}(E_p,x)\,\mathrm{d}E_p$$

10

$$- \int\limits_0^\infty \frac{\partial}{\partial E_p}[E_p\overline{\beta_x}n_{E_p}(E_p,x)]\,\mathrm{d}E_p. \tag{31}$$

Assuming that $n_{E_p}(\infty,x) \to 0$, the second integral in Eq. (31) vanishes and the first integral becomes $N\langle\beta_x\rangle$, where the angle brackets now represent an ensemble average.

In turn, upon applying the product rule to the derivative $\partial[E_p\partial(\overline{\beta_x^2}E_p n_{E_p})/\partial E_p]/\partial E_p$, the second integral in Eq. (30) may be written as

15

$$\frac{mg\cos\theta}{8\tan\phi} \int\limits_0^\infty \frac{\partial}{\partial E_p}\left(E_p\frac{\partial}{\partial E_p}[\overline{\beta_x^2}E_p n_{E_p}(E_p,x)]\right)\mathrm{d}E_p$$

$$- \frac{mg\cos\theta}{8\tan\phi} \int\limits_0^\infty \frac{\partial}{\partial E_p}[\overline{\beta_x^2}E_p n_{E_p}(E_p,x)]\,\mathrm{d}E_p. \tag{32}$$

Assuming that $n_{E_p}(\infty,x) \to 0$ and $\partial n_{E_p}/\partial E_p|_{E_p\to\infty} \to 0$, the integrals in Eq. (32) reduce to $(mg\cos\theta/8\tan\phi)\overline{\beta_x^2}E_p n_{E_p}(0,x)$ with $\overline{\beta_x^2}E_p = 0$ when evaluated at $E_p = 0$. Thus, whereas the diffusive term in Eq. (18) redistributes energy by modifying the

20 density $n_{E_p}(E_p,x)$ (see below), it does not contribute to the total energy balance. The second integral in Eq. (17) is thus

$$\int\limits_0^\infty E_p K_c(E_p,x)\,\mathrm{d}E_p = -\frac{Nmg\langle\beta_x\rangle\cos\theta}{4\tan\phi}. \tag{33}$$

We return to these results below.

3.3.5 Energy loss with deposition

For illustration, suppose initially (unrealistically) that deposition is independent of the particle energy state E_p. This means that the number of particles disentrained within any small energy interval E_p to $E_p + \mathrm{d}E_p$ is a fixed proportion k_3 of the particles within this interval. Thus, $K_d(E_p, x) = -k_d n_{E_p}(E_p, x)$ and the third integral in Eq. (17) becomes

$$5 \quad -k_d \int_0^\infty E_p n_{E_p,x}(E_p, x)\,\mathrm{d}E_p = -k_d E(x). \tag{34}$$

If we momentarily assume that no heating or cooling occurs, then $\mathrm{d}E(x)/\mathrm{d}x = -k_d E(x)$. The solution of this is $E(x) = E(0)e^{-k_d x}$, where $E(0)$ denotes the starting energy at $x = 0$. That is, the total energy $E(x)$ decays exponentially with downslope position x. In this example, note that the form of the density $n_{E_p}(E_p, x)$ is immaterial. Moreover, as a point of reference we may momentarily equate the left side of Eq. (18) with the last term in this equation and write

$$10 \quad \int_0^\infty \frac{\partial n_{E_p}(E_p, x)}{\partial x}\,\mathrm{d}E_p = -k_d \int_0^\infty n_{E_p}(E_p, x)\,\mathrm{d}E_p. \tag{35}$$

This yields $(1/N)\mathrm{d}N/\mathrm{d}x = -k_d$. With $\mathrm{d}E(x)/\mathrm{d}x = -k_d E(x) = -k_d N\langle E_p \rangle$, then $\mathrm{d}E(x)/\mathrm{d}x = \langle E_p \rangle \mathrm{d}N/\mathrm{d}x$. Thus, comparing this result with Eq. (12), the situation in which deposition is independent of the particle energy state is consistent with isothermal conditions wherein the average energy state is unchanging, that is, $\mathrm{d}\langle E_p \rangle/\mathrm{d}x = 0$.

More generally, deposition is unlikely to be independent of the particle energy state, as particles with small energy are
15 on average more likely to become disentrained than are particles with large energy. Thus, $K_d(E_p, x)$ likely possesses a more complicated form than in the example above. Whereas early work on granular gases focused on their behavior in the absence of deposition, the phenomenon of thermal collapse, condensation and freezing in a gravitational field now is receiving significant attention (Volfson et al., 2006; Kachuck and Voth, 2013). We can lean on insight from this work, but because energy dissipation in a granular gas is dominated by particle-particle collisions rather than particle-boundary collisions, the rarefied problem
20 considered here is quite different. As with approaches used in the study of condensation and freezing of granular gases, our analysis at this stage is aimed at lowest order behavior.

For any position x, we do not know the ensemble distribution $f_{E_p}(E_p, x)$ of particle energy states E_p with expected value $\langle Ep \rangle$. Because no particle can be heated to an energy greater than $E_p(0) + mg\sin\theta x$ (representing a complete conversion of gravitational to kinetic energy without any loss due to particle-surface collisions), we know only that $0 \le E_p \le E_p(0) +$
25 $mg\sin\theta x$. Most energies likely are significantly smaller than the upper limit due to collisions.

Collecting results from above, the density $n_{E_p}(E_p, x)$ satisfies a Fokker-Planck-like equation, namely,

$$\frac{\partial n_{E_p}(E_p, x)}{\partial x} = -mg\sin\theta \frac{\partial n_{E_p}(E_p, x)}{\partial E_p}$$

$$+\frac{mg\overline{\beta_x}\cos\theta}{4\tan\phi} \frac{\partial n_{E_p}(E_p, x)}{\partial E_p}$$

$$+\frac{mg\overline{\beta_x^2}\cos\theta}{8\tan\phi}\frac{\partial^2}{\partial E_p^2}[E_p n_{E_p}(E_p,x)]$$

$$-K_d(E_p,x)\,, \tag{36}$$

where we are assuming for simplicity that $\overline{\beta_x}$ and $\overline{\beta_x^2}$ are fixed. As a reminder, the first term on right side of Eq. (36) represents gravitational heating, and the second and third terms on the right side represent frictional cooling. The term $-K_d(E_p,x)$, which describes the loss of energy associated with deposition, is defined below.

Let $n_{E_{p0}}$ and E_{p0} denote suitable characteristic values of the density n_{E_p} and the energy E_p, and let X denote a characteristic length scale. We now define the following dimensionless quantities denoted by circumflexes:

$$n_{E_p}=n_{E_{p0}}\hat{n}_{E_p}\,,\quad E_p=E_{p0}\hat{E}_p \quad\text{and}\quad x=X\hat{x}\,. \tag{37}$$

Upon substituting these quantities into Eq. (36), we may identify three characteristic length scales, namely,

$$X=X_h=\frac{E_{p0}}{mg\sin\theta}\,, \tag{38}$$

$$X=X_{cA}=\frac{4E_{p0}\tan\phi}{mg\overline{\beta_x}\cos\theta}=\frac{\lambda}{\overline{\beta_x}}\quad\text{and} \tag{39}$$

$$X=X_{cD}=\frac{8E_{p0}\tan\phi}{mg\overline{\beta_x^2}\cos\theta}=\frac{2\lambda}{\overline{\beta_x^2}}\,. \tag{40}$$

The first of these, X_h, represents the distance required to heat a particle to the energy state E_{p0} in the absence of frictional cooling. The second, X_{cA}, represents the distance over which thermal collapse by advective cooling occurs. The third, X_{cD}, represents a distance over which diffusive cooling occurs.

We now define two dimensionless numbers, the Kirkby number[1],

$$Ki=\frac{X_{cA}}{X_h}=\frac{4\tan\phi S}{\overline{\beta_x}} \tag{41}$$

and a cooling Péclet-like number,

$$Pe_c=\frac{X_{cD}}{X_{cA}}=\frac{2\overline{\beta_x}}{\overline{\beta_x^2}}\,. \tag{42}$$

---

[1]This number is named in honor of Michael J. Kirkby for his pioneering work on hillslope processes, including the topic of particle motions on scree surfaces.

The Kirkby number Ki is the ratio of gravitational heating to advective cooling. The Péclet-like number Pe_c is the ratio of advective cooling to diffusive cooling. Choosing X_{cA} as the characteristic length scale and neglecting the deposition term in Eq. (36), we now rewrite it as

$$\frac{\partial \hat{n}_{\hat{E}_p}(\hat{E}_p, \hat{x})}{\partial \hat{x}} = -Ki \frac{\partial \hat{n}_{\hat{E}_p}(\hat{E}_p, \hat{x})}{\partial \hat{E}_p}$$

5

$$+ \frac{\partial \hat{n}_{\hat{E}_p}(\hat{E}_p, \hat{x})}{\partial \hat{E}_p} + \frac{1}{Pe_c} \frac{\partial^2}{\partial \hat{E}_p^2} [\hat{E}_p \hat{n}_{\hat{E}_p}(\hat{E}_p, \hat{x})]. \tag{43}$$

Note that with $\beta_x \ll 1$, then $Pe_c \gg 1$ according to Eq. (42), such that the diffusive term in Eq. (43) becomes insignificant relative to the advective cooling term.

With reference to Figure 3, imagine a great number of particles whose initial energy states at $x = 0$ are described by the
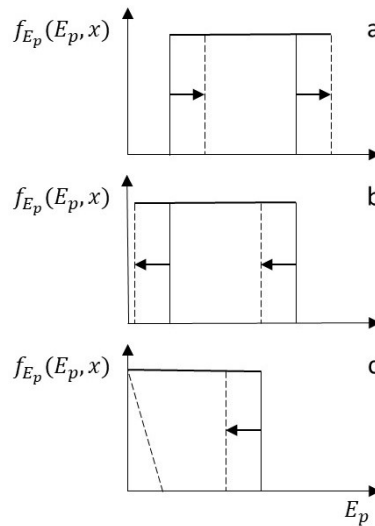
Figure 3. Schematic diagram of downslope changes in the distribution $f_{E_p}(E_p, x)$ of particle energy states E_p (for simplicity a uniform distribution) due to: (a) gravitational advective heating in the absence of cooling; (b) advective frictional cooling in the absence of heating; and (c) net cooling. The triangular region represents an idealized "window" of increasing likelihood of deposition with decreasing particle energy E_p. Note that an effect of deposition is to increase the average energy $\langle E_p \rangle$ by culling lower energy particles, thereby selecting higher energy particles for continued travel with increasing distance.

10 density $n_{E_p}(E_p, 0)$. With just gravitational heating, this distribution is advected to higher energy values at a fixed rate $mg \sin \theta$. With just frictional cooling, but in the absence of diffusion, the distribution is advected to lower energy values at a fixed rate $mg \overline{\beta_x} \cos \theta / 4 \tan \phi$. If gravitational heating is balanced by advective cooling ($Ki = 1$), the form of the distribution remains fixed with increasing distance x. With diffusive cooling, advective cooling of the density $n_{E_p}(E_p, x)$ to lower energy values involves smoothing of this density. When these effects are combined, whether heating is greater than advective cooling ($Ki > 1$)

or vice versa ($Ki < 1$), no value of E_p is larger than $E_p(0) + mg\sin\theta x$, and most values are significantly less than this maximum due to the increasing likelihood of particle-surface interactions (cooling) within increasing x. When the magnitude of the term in Eq. (43) involving Ki is greater than the sum of the magnitudes of the two cooling terms, then net heating occurs. When the magnitudes of the cooling terms are larger than the heating term, then net cooling occurs. For particles reaching relatively

5   small energy states, there is an increasing likelihood of deposition (see below). As a reminder, this description does not pertain to the energy states of a great number of particles during an interval of time. Rather, this description pertains to an ensemble of particles reaching any position x over a long period of time when treated as a cohort. That is, $n_{E_p}(E_p, x)$ is the density of particle energies at any x representing the great number of particles that occupied this position while in motion at many previous instants in time.

10   We now offer a simple hypothesis describing the loss of energy associated with deposition. Recall that X_{cA} is a measure of the distance over which particles with energy E_{p0} thermally collapse by frictional cooling. We may imagine, for example, a sudden removal of the source of heating such that X_{cA} is a measure of the distance of relaxation to a total loss of energy. For particles with energy E_p, this length scale can be expressed more generally as

$$l_c(E_p) \sim \frac{4E_p \tan\phi}{mg\overline{\beta_x}\cos\theta}, \tag{44}$$

15   which becomes unbounded only in the limit of $\theta \to \pi/2$. Because thermal collapse involves deposition, we then assume at lowest order that

$$\alpha l_c(E_p)\frac{\partial n_{E_p}(E_p, x)}{\partial x}\bigg|_d = -n_{E_p}(E_p, x), \tag{45}$$

where the subscript d denotes that the derivative refers to a change in the density $n_{E_p}(E_p, x)$ just associated with deposition. We emphasize that Eq. (45) pertains to the imagined situation in which gravitational heating is not involved. This is the same

20   as assuming a spatial Poisson process of deposition, that is, a fixed disentrainment rate keyed to the specific energy state E_p. In the presence of heating, however, the length scale of deposition increases relative to l_c. That is, heating suppresses the disentrainment rate. The factor α thus modulates the length scale l_c so the product αl_c is a net e-folding length in the presence of heating. As described below, the factor α is assumed to be a function of the Kirkby number.

Substituting Eq. (45) into Eq. (17) and evaluating the integral then yields

25

$$\int_0^\infty E_p \frac{\partial n_{E_p}(E_p, x)}{\partial x}\bigg|_d \, dE_p$$

$$= -\frac{mg\cos\theta}{\alpha 4 \tan\phi}\int_0^\infty \overline{\beta_x} n_{E_p}(E_p, x)\, dE_p$$

$$= -\frac{Nmg\langle\beta_x\rangle\cos\theta}{\alpha 4\tan\phi}, \tag{46}$$

where we now redefine the Kirkby number as

$$Ki = \frac{4\tan\phi S}{\langle\beta_x\rangle}, \tag{47}$$

assuming that $\overline{\beta_x}$ is independent of E_p. Comparing this result with Eq. (33), the energy loss rate due to deposition is the same as the advective cooling rate, but modulated by the factor α.

5   3.4   Conservation of mass revisited

The preceding provides the basis for separately calculating the disentrainment rate, consistent with the deposition rate. Because $n_{E_p}(E_p, x)\mathrm{d}E_p$ represents the number of particles within the small energy interval E_p to $E_p + \mathrm{d}E_p$, using Eq. (44) and Eq. (45) the total disentrainment rate is therefore

$$\frac{\mathrm{d}N(x)}{\mathrm{d}x} = \int_0^\infty \frac{\partial n_{E_p}(E_p, x)}{\partial x}\,\mathrm{d}E_p$$

10

$$= -\frac{mg\langle\beta_x\rangle\cos\theta}{\alpha 4\tan\phi}\int_0^\infty \frac{1}{E_p} n_{E_p}(E_p, x)\,\mathrm{d}E_p$$

$$= -\frac{Nmg\langle\beta_x\rangle\cos\theta}{\alpha 4\tan\phi}\left\langle\frac{1}{E_p}\right\rangle. \tag{48}$$

Thus, the deposition rate is proportional to the cooling rate, as it should be. Here it is important to note that the expected value
15    $\langle 1/E_p\rangle \neq 1/\langle E_p\rangle$. In fact, $\langle 1/E_p\rangle$ is the reciprocal of the harmonic mean (Appendix F). This means that $\langle E_p\rangle\langle 1/E_p\rangle \geq 1$. Only in the limit where $n_{E_p}(E_p, x)$ has zero variance does $\langle 1/E_p\rangle \to 1/\langle E_p\rangle$. To simplify the notation, hereafter we denote the arithmetic mean as $\langle E_p\rangle = E_a$ and the harmonic mean as $1/\langle 1/E_p\rangle = E_h$. Thus $E_a/E_h \geq 1$.

As a point of reference we may now define an ensemble averaged deposition length as

$$L_c \sim \frac{\alpha 4\tan\phi E_h}{mg\langle\beta_x\rangle\cos\theta} = \frac{\alpha E_h}{mg\mu\cos\theta}, \tag{49}$$

20   with $\mu = \langle\beta_x\rangle/4\tan\phi$. Note that in contrast to the energy specific length scale l_c in Eq. (44) and Eq. (45), L_c in Eq. (49) is keyed to the harmonic average energy of the ensemble. Setting $\theta = 0$ so that $\cos\theta = 1$, the length scale L_c is entirely analogous to the length scale λ_0 used by Furbish and Haff (2010), Furbish and Roering (2013) and Doane et al. (2018) as the characteristic particle travel distance on a flat surface, thence modulated with increasing slope S (see also Section 5.3).

The factor α has a key role in the formulation. As described above, this factor modulates the length scale L_c in the presence
25   of gravitational heating. Note that Eq. (48) is equivalent to

$$L_c\frac{\mathrm{d}N}{\mathrm{d}x} = -N. \tag{50}$$

For a given value of α the length scale L_c is set by the cooling rate, and this length scale increases with increasing slope angle θ. But gravitational heating also increases with θ, the effect of which is to suppress the rate of deposition and increase L_c.

That is, the deposition length scale is not the same as the cooling length scale. As described below, whereas l_c is a measure of the rate of extraction of translational energy, this includes its conversion to rotational energy whose effect is to decrease the likelihood of stopping. On dimensional grounds an inspired guess suggests that this effect is a function $f(Ki)$ of the Kirkby number Ki. For example, suppose that

$$L_c = \frac{\alpha E_h}{mg\mu\cos\theta} = \frac{\alpha_0 E_h}{mg\mu\cos\theta - mg\mu_1\sin\theta} \,. \tag{51}$$

where μ_1 is a coefficient of order unity. This leads to

$$\alpha = \frac{\alpha_0}{1 - \mu_1 Ki} \,, \tag{52}$$

where $\alpha \to \alpha_0$ as $\mu_1 Ki \to 0$. Now,

$$L_c = \frac{\alpha_0 E_h}{mg\mu\cos\theta(1 - \mu_1 Ki)} \,. \tag{53}$$

This example suggests that $L_c \to \infty$ as $\mu_1 Ki \to 1$. That is, $\mu_1 Ki \to 1$ sets an upper limit above which deposition is insignificant. More generally we may write

$$L_c = \frac{\alpha_0 f(Ki) E_h}{mg\mu\cos\theta} \,, \tag{54}$$

to indicate the possibility of other dependencies of α on Ki. Note that we provide evidence for this behavior in the companion paper, including the form of Eq. (52) based on experiments. For notational simplicity in subsequent sections, we use α with the understanding that this implies $\alpha = \alpha_0 f(Ki)$.

Here is a key sidebar for reference in our descriptions below of related formulations. We emphasize that according to Eq. (45) and Eq. (48) the deposition rate is proportional to the advective cooling rate rather than the net cooling rate (the difference between the rates of heating and cooling), where the rate of heating then modulates the deposition rate, therein increasing the deposition length scale. Moreover, the deposition rate explicitly depends on the energy state of the particles. Consider a thought experiment. Let us imagine a system consisting of a box containing a finite number of particles. Suppose that we mechanically add energy to the system such that some proportion of the particles becomes a rarefied granular gas, and suppose that the gas achieves a non-equilibrium steady state with a specific average energy state (Appendix G). This means that the rate of (mechanical) heating is equal to the rate of cooling due to dissipative particle-box collisions, and sublimation (entrainment) matches deposition (disentrainment). That is, depending on the energy state of the particles, deposition occurs even though the difference between the rate of heating and cooling is zero. Now imagine that when a particle is deposited, it cannot become re-entrained. The rate of heating and cooling of the remaining gas particles is still the same, yet the deposition process continues for those particles which, by chance, cool to sufficiently low energies for deposition to occur — just as deposition of these particles would have occurred before re-entrainment was "turned off." Furthermore, the average energy of the gas (active) particles can remain fixed while their total energy decreases due to irreversible deposition. Thus, we are assuming that the deposition rate is proportional to the cooling rate rather than the net cooling rate, depending on the energy state of the particles. The effect of heating is to decrease the likelihood of deposition by decreasing the proportion of particles that cool to sufficiently

20

low energies for deposition to occur — which translates to suppressing the disentrainment rate and increasing the length scale of deposition.

3.5 Energy and mass balances

With $\mu = \langle \beta_x \rangle / 4 \tan \phi$ we now collect results from above. The total energy balance is given by

$$\frac{\mathrm{d}E(x)}{\mathrm{d}x} = Nmg \sin \theta$$

$$-Nmg\mu \cos \theta - \frac{1}{\alpha} Nmg\mu \cos \theta. \tag{55}$$

To summarize, the first term on the right side of Eq. (55) is due to gravitational heating, the second term is due to frictional cooling, and the last term represents a loss of energy due to deposition. Note that none of these terms explicitly involves the energy $E(x)$. In turn, conservation of mass is given by

$$\frac{\mathrm{d}N(x)}{\mathrm{d}x} = -\frac{1}{\alpha} Nmg\mu \cos \theta \frac{1}{E_h}. \tag{56}$$

This is coupled with Eq. (55) via the relation between the total energy $E(x)$, the average energy E_a and the harmonic average energy E_h (see below), and the explicit appearance of N in both of these equations.

At this point we emphasize that the quantity $\mu = \langle \beta_x \rangle / 4 \tan \phi$ is *not* to be interpreted as Coulomb-like dynamic friction coefficient. Indeed, the product $mg\mu \cos \theta$ in Eq. (55) and Eq. (56) looks like an ordinary Coulomb friction force (e.g., Kirkby and Statham, 1975; Gabet and Mendoza, 2012). Recall, however, that $\cos \theta$ enters from the geometry of particle motions, and does not represent the angle needed to specify the normal component of the weight mg. Similarly, $\tan \phi$ is an expected reflection angle, not a friction angle. We elaborate these points below.

To close the circle in reference to our stating point, Eq. (12), we now combine Eq. (12), Eq. (55) and Eq. (56) to give

$$\frac{\mathrm{d}E_a(x)}{\mathrm{d}x} = mg \sin \theta - mg\mu \cos \theta$$

$$+ \frac{mg\mu \cos \theta}{\alpha} \left(\frac{E_a}{E_h} - 1 \right). \tag{57}$$

This balance involving the average energy E_a rather than the total energy E reveals an important behavior associated with deposition, centered on the parenthetical part of the last term. Namely, it is straightforward to show (Appendix F) that $E_a/E_h - 1 \geq 0$. The last term in Eq. (57) therefore represents an apparent heating associated with deposition. With reference to Figure 3, a net advective cooling uniformly lowers all particle energy states, thus lowering the average energy E_a as well as the total energy E. As this cooling lowers all energy states, some particles enter the range where deposition occurs, and the deposition rate therefore is proportional to the net advective cooling rate. In the absence of a net advective cooling, particles with small

energy nonetheless are preferentially disentrained, so the average energy state increases. When cooling and deposition are combined, the average energy decreases more slowly than it otherwise would in the absence of deposition. This effect increases with increasing variance in the distribution of energies (Appendix F), and it vanishes as the variance goes to zero. The balance described by Eq. (57) thus provides a formal description of what we intuitively know: deposition culls lower energy particles,

5   thereby selecting higher energy particles for continued travel with increasing distance. We note that Brilliantov et al. (2018) demonstrate an analogous unexpected behavior of granular gases, namely, the heating of a granular gas associated with particle aggregation with continued loss of total energy. This occurs when the rate of loss of particles by aggregation exceeds the rate of loss of total energy, such that by definition the average particle energy increases.

The balance described by Eq. (57) also reveals an important constraint on particle energies. Namely, if we imagine the

10   special situation of isothermal conditions ($\mathrm{d}E_a/\mathrm{d}x = 0$), then frictional cooling given by the second term on the right side of Eq. (57) must balance two sources of heating, namely, the first and third terms on the right side. This requires that either the Kirkby number $Ki < 1$ or, if $Ki = 1$, then the distribution $f_{E_p}(E_p, x)$ of energies E_p must have zero variance such that $E_h = E_a$. Because this latter condition is highly unlikely, an isothermal condition generally requires that $Ki < 1$. Conversely, net heating must occur with $Ki > 1$.

15   According to Eq. (55) or Eq. (57), for a given slope angle θ the spatial rate of net cooling (or net heating) of the ensemble is a fixed quantity in which this slope angle has a dual role. Namely, an increasing slope decreases the rate of frictional cooling by decreasing the expected occurrence of particle-surface collisions, and it simultaneously increases the rate of gravitational heating. With $\theta = 0$, heating vanishes and frictional cooling occurs at a maximum rate of $\mu m g$. In turn, as $\theta \to \pi/2$, which represents a vertical cliff, frictional cooling vanishes and heating matches that of free-fall motion. This transition from small

20   to large slopes nicely illustrates what virtually every undergraduate student learns intuitively from the sport of boulder rolling (or "trundling" (Forrester, 1931)), and why this sport is so spectacular and satisfying in steep terrain. Moreover, recall that the Kirkby number $Ki = S/\mu$ is the ratio of gravitational heating to advective cooling. If these are balanced, $Ki = 1$ and

$$S = \mu = \frac{\langle \beta_x \rangle}{4 \tan \phi}. \tag{58}$$

Qualitatively, this is the slope at which an undergraduate student may expect that boulder rolling starts to become particularly

25   interesting.

The formulation also nicely illustrates that if the heating and cooling rates are matched, this does not imply an absence of deposition, as the last terms in Eq. (55) and Eq. (57) may be finite with $Ki = 1$. Moreover, because this is a probabilistic phenomenon, some particles are likely to become disentrained even on steep, rough slopes where heating on average exceeds cooling. Experienced undergraduates indeed inform us that some boulders just do not make it all the way to the bottom of the

30   hillslope despite their best efforts to select conditions satisfying $Ki > 1$.

4 General behavior

4.1 Effects of energy balance

There is value in restating Eq. (55), Eq. (56) and Eq. (57) in dimensionless form. Let E_{a0} denote the initial average particle energy at $x = 0$ and let N_0 denote the initial number of particles at $x = 0$. In turn we define a characteristic cooling distance

5   $X = E_{a0}/mg\mu\cos\theta$ so that $E_{a0} = mg\mu\cos\theta X$. We now define the following dimensionless quantities denoted by circum-flexes:

$$x = X\hat{x}, \quad N = N_0\hat{N}, \quad E = N_0 E_{a0}\hat{E},$$

$$E_a = E_{a0}\hat{E}_a \quad \text{and} \quad E_h = E_{a0}\hat{E}_h. \tag{59}$$

10   With these definitions we write Eq. (55), Eq. (56) and Eq. (57) as

$$\frac{\mathrm{d}\hat{E}(\hat{x})}{\mathrm{d}\hat{x}} = \left[Ki - \left(1 + \frac{1}{\alpha}\right)\right]\hat{N}, \tag{60}$$

$$\frac{\mathrm{d}\hat{N}(\hat{x})}{\mathrm{d}\hat{x}} = -\frac{\hat{N}}{\alpha\hat{E}_h} \quad \text{and} \tag{61}$$

15   $$\frac{\mathrm{d}\hat{E}_a(\hat{x})}{\mathrm{d}\hat{x}} = Ki - 1 + \frac{1}{\alpha}\left(\frac{\hat{E}_a}{\hat{E}_h} - 1\right). \tag{62}$$

Because the dimensionless disentrainment rate $\hat{P}_{\hat{x}}(\hat{x}) = -(1/\hat{N})\mathrm{d}\hat{N}/\mathrm{d}\hat{x}$, notice that Eq. (61) provides the basis for determining the distribution of travel distances using Eq. (4). This requires specifying how $\hat{E}_h$ varies with $\hat{x}$ for given values of α and Ki. At this point, however, we must confront the fact that we have four unknowns, $\hat{N}$, $\hat{E}$, $\hat{E}_a$ and $\hat{E}_h$, and three equations, one of which is nonlinear in the ratio $\hat{E}_a/\hat{E}_h$. Here we add a fourth equation by assuming that this ratio remains fixed, namely,

20

$$\frac{\hat{E}_a}{\hat{E}_h} = \gamma. \tag{63}$$

We do not know the distribution $f_{\hat{E}_p}(\hat{E}_p)$ required to determine γ (Appendix F). Nonetheless, Eq. (63) essentially assumes that the form of $f_{\hat{E}_p}(\hat{E}_p)$ remains similar with distance $\hat{x}$. This allows us to illustrate key elements of the formulation.

With the assumption of Eq. (63) we note that Eq. (61) becomes

25   $$\frac{\mathrm{d}\hat{N}(\hat{x})}{\mathrm{d}\hat{x}} = -\frac{\gamma\hat{N}}{\alpha\hat{E}_a}, \tag{64}$$

and Eq. (62) becomes

$$\frac{\mathrm{d}\hat{E}_a(\hat{x})}{\mathrm{d}\hat{x}} = Ki - 1 + \frac{1}{\alpha}(\gamma - 1). \tag{65}$$

Focusing initially on Eq. (65), isothermal conditions exist if $\mathrm{d}\hat{E}_a/\mathrm{d}\hat{x} = 0$. We then rearrange Eq. (62) or Eq. (65) to define a transition value of the Kirkby number, namely,

$$5 \quad Ki_* = 1 - \frac{1}{\alpha}\left(\frac{\hat{E}_a}{\hat{E}_h} - 1\right) = 1 - \frac{1}{\alpha}(\gamma - 1). \tag{66}$$

If $Ki < Ki_*$ then cooling occurs ($\mathrm{d}\hat{E}_a/\mathrm{d}\hat{x} < 0$); and if $Ki > Ki_*$ then heating occurs ($\mathrm{d}\hat{E}_a/\mathrm{d}\hat{x} > 0$). Recall that $\hat{E}_a/\hat{E}_h = \gamma \geq 1$ (Appendix F) so that $\gamma - 1 \geq 0$. If the variance of energy states E_p is zero then $\hat{E}_a/\hat{E}_h = \gamma = 1$ giving $Ki_* = 1$. Thus, in this case cooling occurs with $Ki < 1$ and heating occurs with $Ki > 1$. The ratio $\hat{E}_a/\hat{E}_h = \gamma$ generally increases with the variance of E_p, thus decreasing Ki_*. That is, as this variance increases, the transition between cooling and heating occurs at

10 a smaller value of the Kirkby number. This represents a stronger culling (deposition) of lower energy particles. The largest possible transition value is $Ki_* = 1$.

We now start with an idealized example that illustrates key elements of the formulation, including the coupling between Eq. (60), Eq. (61) and Eq. (62). Assume that the Kirkby number Ki is fixed, and assume isothermal conditions. Thus $\mathrm{d}\hat{E}_a/\mathrm{d}\hat{x} = 0$ with $\hat{E}_a = \hat{E}_{a0}$ so that Eq. (62) leads to

$$15 \quad \hat{E}_h = \frac{\hat{E}_{a0}}{1 + \alpha(1 - Ki)}. \tag{67}$$

With $\hat{E}_a/\hat{E}_h = \hat{E}_{a0}/\hat{E}_h = \gamma$, then $\gamma = 1 + \alpha(1 - Ki)$. The disentrainment rate $\hat{P}_{\hat{x}}(\hat{x}) = -(1/\hat{N})\mathrm{d}\hat{N}/\mathrm{d}\hat{x}$. Thus, according to Eq. (61) and Eq. (67),

$$\hat{P}_{\hat{x}}(\hat{x}) = \frac{1 + \alpha(1 - Ki)}{\alpha\hat{E}_{a0}} = \frac{\gamma}{\alpha\hat{E}_{a0}}. \tag{68}$$

In turn, using Eq. (4) this yields an exponential distribution of travel distances with mean

$$20 \quad \mu_{\hat{x}} = \frac{\alpha\hat{E}_{a0}}{1 + \alpha(1 - Ki)} = \frac{\alpha\hat{E}_{a0}}{\gamma}, \tag{69}$$

so that

$$\hat{N}(\hat{x}) = \frac{1}{\mu_{\hat{x}}}e^{-\hat{x}/\mu_{\hat{x}}}. \tag{70}$$

Note that an increasing value of γ in Eq. (69) represents an increasing proportion of lower energy particles available for deposition relative to this availability with $\gamma \to 1$, the effect of which is to decrease the mean travel distance.

25 The total energy $\hat{E}$ also declines exponentially with $\hat{x}$. Namely, substituting Eq. (70) into Eq. (60) leads to

$$\hat{E}(\hat{x}) = 1 - \frac{1}{\alpha}[1 + \alpha(1 - Ki)](1 - e^{-\hat{x}/\mu_{\hat{x}}})$$

$$= 1 - \frac{\gamma}{\alpha}(1 - e^{-\hat{x}/\mu_{\hat{x}}}). \tag{71}$$

This example of isothermal conditions illustrates that with $\hat{E}_a = \hat{E}_{a0}$, then according to Eq. (69) the average travel distance $\mu_{\hat{x}}$ is directly proportional to the initial average energy. However, isothermal conditions are unlikely, because according to
5 Eq. (66), such a condition requires a specific value of Ki for the ratio $\hat{E}_a/\hat{E}_h = \gamma$. We now consider the more general case involving either net cooling or net heating.

As above we assume that the ratio $\hat{E}_a/\hat{E}_h = \gamma$ is fixed, although the averages $\hat{E}_a$ and $\hat{E}_h$ otherwise are unconstrained. Net cooling or net heating is not prescribed; either condition is allowed. Using Eq. (60) and Eq. (61) the disentrainment rate is (Appendix H)

10 $$\hat{P}_{\hat{x}}(\hat{x}) = \frac{1}{a\hat{x} + b}, \tag{72}$$

where

$$a = \frac{\alpha}{\gamma}\left(Ki - 1 + \frac{\gamma}{\alpha} - \frac{1}{\alpha}\right) = \frac{\alpha}{\gamma}(Ki - Ki_*) \quad \text{and}$$

$$b = \frac{\alpha \hat{E}_{a0}}{\gamma}. \tag{73}$$

15 Note that as $a \to 0$ the disentrainment rate goes to a fixed value equal to $1/b = \gamma/\alpha\hat{E}_{a0}$, and the distribution $f_{\hat{x}}(\hat{x})$ of travel distances $\hat{x}$ goes to an exponential distribution with mean $\mu_{\hat{x}} = b = \alpha\hat{E}_{a0}/\gamma$. A value of $a > 0$ ($Ki > Ki_*$) implies decreasing disentrainment with increasing x. A value of $a < 0$ ($Ki < Ki_*$) implies increasing disentrainment.

More generally, the distribution of travel distances is a generalized Pareto distribution with position parameter equal to zero (Appendix H), namely,

20 $$f_{\hat{x}}(\hat{x}) = \frac{b^{1/a}}{(a\hat{x} + b)^{1+1/a}}, \tag{74}$$

where now $a \in \Re$ is interpreted as a shape parameter and $b > 0$ is a scale parameter (Pickands, 1975; Hosking and Wallis, 1987). The cumulative distribution is

$$\hat{F}_{\hat{x}}(\hat{x}) = \begin{cases} 1 - \dfrac{b^{1/a}}{(a\hat{x}+b)^{1/a}} & a \neq 0 \\ 1 - e^{-\hat{x}/b} & a = 0, \end{cases} \tag{75}$$

and the exceedance probability is

25 $$\hat{R}_{\hat{x}}(\hat{x}) = \begin{cases} \dfrac{b^{1/a}}{(a\hat{x}+b)^{1/a}} & a \neq 0 \\ e^{-\hat{x}/b} & a = 0. \end{cases} \tag{76}$$

For $a < 1$ the mean is

$$\mu_{\hat{x}} = \frac{b}{1-a} = \frac{\alpha \hat{E}_{a0}}{1 + \alpha - \alpha Ki}, \tag{77}$$

which is independent of the ratio $\gamma = \hat{E}_a / \hat{E}_h$. This is the same as Eq. (69) for isothermal conditions, although the denominator in Eq. (77) generally is not equal to γ. In turn, Eq. (77) requires that

$$Ki < 1 + \frac{1}{\alpha}, \tag{78}$$

which provides the upper limit of Ki for which the mean $\mu_{\hat{x}}$ is defined. Because $\alpha > 0$, this limit may be greater than one. For $a < 1/2$ the variance is

$$\sigma_{\hat{x}}^2 = \frac{b^2}{(1-a)^2(1-2a)}$$

$$= \frac{\alpha^2 \hat{E}_{a0}^2}{(1 + \alpha - \alpha Ki)^2 (2/\gamma + 2\alpha/\gamma - 1 - 2\alpha Ki/\gamma)}. \tag{79}$$

Unlike the mean, the variance depends on $\gamma = \hat{E}_a / \hat{E}_h$. In turn, for $a \geq 1$ such that

$$Ki \geq 1 + \frac{1}{\alpha}, \tag{80}$$

the mean of $f_{\hat{x}}(\hat{x})$ is undefined. Moreover, for $a \geq 1/2$ the variance is undefined. These results reflect the heavy-tailed behavior of the generalized Pareto distribution.

As a point of reference in the second companion paper (Furbish et al., 2020a), the generalized Pareto distribution defined by Eq. (74) also may be considered a generalized Lomax distribution. This distribution can be rewritten as an ordinary Lomax distribution (Appendix H). Namely, if we define the shape parameter $a_L = 1/a$ and the scale parameter $b_L = b/a$, then Eq. (74) becomes

$$f_{\hat{x}}(\hat{x}) = \frac{a_L b_L^{a_L}}{(\hat{x} + b_L)^{1+a_L}} \qquad a_L, b_L > 0, \tag{81}$$

which is a Lomax distribution with mean

$$\mu_{\hat{x}} = \frac{b_L}{a_L - 1} \qquad a_L > 1. \tag{82}$$

For $a_L > 0$ ($a > 0$) the forms and behaviors of Eq. (74) and Eq. (81) are identical. Notice, however, that if $a < 0$ then $a_L = 1/a < 0$ and $b_L = b/a < 0$ for positive b. This means that we cannot use the form of the Lomax distribution given by Eq. (81) to examine conditions involving $a < 0$. Yet these conditions are mechanically meaningful, so we proceed using the generalized Pareto distribution given by Eq. (74). To be clear, the ordinary Pareto distribution that is normally referred to in the literature is a special case of the generalized Pareto distribution. In turn the Lomax distribution is a special case of the Pareto distribution (and therefore of the generalized Pareto) with position parameter equal to zero.
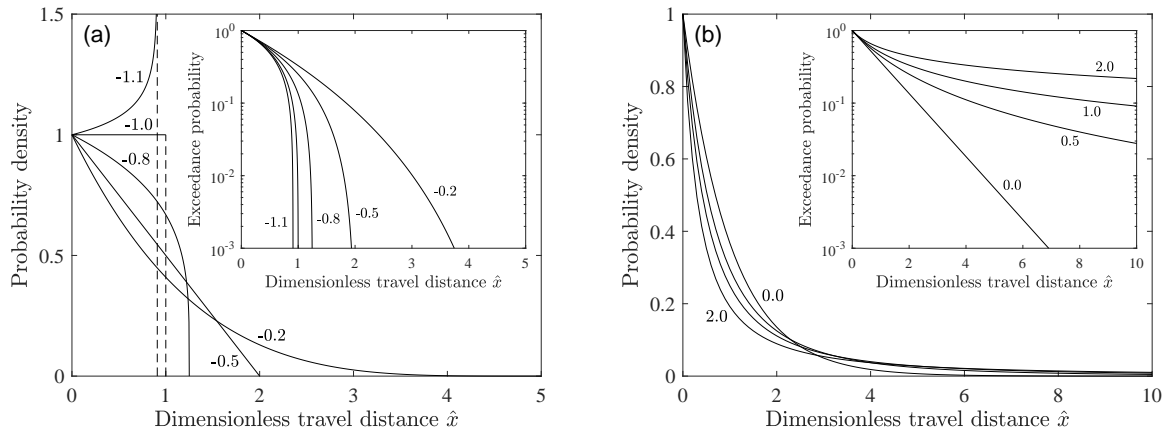
Figure 4. Plot of probability density $f_r(r;x)$ versus travel distance r for scale parameter $B = 1$ and different values of the shape parameter A for (a) $A < 0$ and (b) $A \geq 0$ with associated exceedance probability plots (insets). Figure reproduced from companion paper (Furbish et al., 2020a). Compare with Figure 1 in Hosking and Wallis (1987).

With reference to Figure 4, for $a < 0$ the distribution $f_{\hat{x}}(\hat{x})$ is bounded at a value of $\hat{x} = b/|a|$ with a mean given by Eq. (77). This represents a condition of rapid thermal collapse. Specifically, when $a < -1$ this distribution monotonically increases and becomes asymptotically unbounded at $\hat{x} = b/|a|$. In the limit of $a \to -1$ it becomes a uniform distribution. When $a = -1/2$ this distribution is triangular. For $-1/2 < a < 0$ this distribution decays more rapidly than an exponential distribution and is bounded at the position $\hat{x} = b/|a|$. For $a = 0$, $f_{\hat{x}}(\hat{x})$ becomes an exponential distribution, representing an isothermal condition as described above. For $a > 0$ the distribution $f_{\hat{x}}(\hat{x})$ is heavy-tailed. This represents a condition of net heating. Specifically, for $0 < a < 1/2$ this distribution decays more slowly than an exponential distribution, but it possesses a finite mean and a finite variance. For $1/2 \leq a < 1$ the distribution possesses a finite mean but its variance is undefined. For $a \geq 1$ the mean and variance of $f_{\hat{x}}(\hat{x})$ are both undefined, even though this distribution properly integrates to unity. For $a > 0$ the tail of $f_{\hat{x}}(\hat{x})$ decays as a power function, namely, $f_{\hat{x}}(\hat{x}) \sim \hat{x}^{-(1+1/a)}$. The exceedance probability decays as $R_{\hat{x}}(\hat{x}) \sim \hat{x}^{-1/a}$. These results are summarized in Table 1. We provide evidence of all three behaviors — rapid thermal collapse, isothermal conditions, and net heating — in our second companion paper (Furbish et al., 2020a).

The formulation above assumes uniform surface conditions, specifically, uniform slope angle and roughness texture. We show below (Section 6) how it may be adapted to varying downslope conditions. We also note that the distribution $f_{\hat{x}}(\hat{x})$ given by Eq. (74) can be incorporated into a mixed distribution. Indeed, a mixed distribution is the natural choice for describing the travel distances of a mixture of particle sizes, each involving a different frictional cooling behavior for a given surface roughness (Roth et al., 2020).

Table 1. Behavior of the generalized Pareto distribution associated with the shape parameter a and Kirkby number Ki as illustrated in Figure 4.

Behavior	Range of a	Range of Ki	Mean $\mu_{\hat{x}}$	Variance $\sigma_{\hat{x}}^2$
Bounded[1], increasing with $\hat{x}$	$a < -1$	$Ki < 1 - (2\gamma - 1)/\alpha$	$b/(1-a)$	$b^2/(1-a)^2(1-2a)$
Uniform	$a = -1$	$Ki = 1 - (2\gamma - 1)/\alpha$	$b/2$	$b^2/12$
Bounded[1,2], decreasing with $\hat{x}$	$-1 < a < 0$	$Ki < Ki_* = 1 - (\gamma - 1)/\alpha$	$b/(1-a)$	$b^2/(1-a)^2(1-2a)$
Exponential	$a = 0$	$Ki = Ki_* = 1 - (\gamma - 1)/\alpha$	b	b^2
Finite mean and variance	$0 < a < 1/2$	$Ki_* < Ki < Ki_* + \gamma/2\alpha$	$b/(1-a)$	$b^2/(1-a)^2(1-2a)$
Finite mean, undefined variance	$1/2 \le a < 1$	$Ki_* + \gamma/2\alpha \le Ki < 1 + 1/\alpha$	$b/(1-a)$	—
Undefined mean and variance	$a \ge 1$	$Ki \ge 1 + 1/\alpha$	—	—

[1] Truncation occurs at dimensionless distance $\hat{x} = b/|a|$.

[2] Triangular with $a = -1/2$

4.2 Elements of the average travel distance

The average travel distance given by Eq. (77) for $Ki < 1 + 1/\alpha$ contains all of the elements that influence particle motions except the quantity γ. Thus, whereas the average by itself does not reveal the source of variations in the form of distribution of travel distances, Eq. (74), the average nonetheless provides a focal point. Here we rewrite this average in its dimensional form, then step through the significance of its elements. Namely, with $E_{a0} = (1/2)m\langle u_0^2 \rangle$ and $Ki = S/\mu = (1/\mu)mg\sin\theta/mg\cos\theta$,

$$\mu_x = \frac{E_{a0}}{mg\mu\cos\theta}\frac{\alpha}{1 + \alpha - \alpha Ki}$$

$$= \frac{E_{a0}}{(1 + 1/\alpha)mg\mu\cos\theta - mg\sin\theta}. \tag{83}$$

For an ensemble of particles whose motions start at $x = 0$, the average travel distance μ_x increases directly with the average starting energy $E_{a0} \propto \langle u_0^2 \rangle$. This is entirely akin to the formulation by Kirkby and Statham (1975) (see below), and it highlights the significance of the initial particle energy conditions at $x = 0$ in setting their travel distances. The archetypal example involves rock fall from cliffs followed by their motions over talus and scree slope surfaces (Figure 1), where fall heights and initial rebounds set the initial average downslope energy. This also is a key element in experiments where initial energies are set by the choice of drop height (Kirkby ana Statham, 1975) or launch speed (Gabet and Mendoza, 2012; DiBiase et al., 2017). This aspect of the formulation also points to the significance of energetics associated with the entrainment rate $E_s(x)$ in Eq. (5) and Eq. (6) at hillslope positions that are not necessarily as well-defined as, say, the base of a cliff (see Section 6).

The average travel distance μ_x is inversely proportional to the rate of frictional cooling represented by $\mu g\mu\cos\theta$. Here we reemphasize that despite its form, this expression does not represent a Coulomb-like friction. Rather, this expression enters the formulation via the characteristic length λ in setting the expected number of collisions per unit distance, n_x. As described below, the surface-normal component of the particle weight does not set collisional friction; this is set by dynamic forces during

collisions. Moreover, the appearance of the Kirkby number Ki in the denominator of Eq. (83) indicates that as Ki increases, the denominator becomes smaller (subject to the conditions that $Ki < 1 + 1/\alpha$), so the average travel distance increases. We also note that, except for purely bouncing motions, it is incorrect to interpret the length λ strictly as a saltation-like distance. This is a scaling approximation (Appendix D) to show that n_x must involve the average energy ($\propto \langle u^2 \rangle$) and the geometrical

5   factor $\cos\theta$ at lowest order.

Notice that Eq. (83) indicates that with $E_{a0} = (1/2)m\langle u_0^2 \rangle$ the average travel distance μ_x is independent of the particle mass m. Viewed in isolation, this suggests that large particles should on average travel no farther than small particles. However, this is inconsistent with what is observed in laboratory and field-based experiments (Kirkby and Statham, 1975; DiBiase et al., 2017; Roth et al., 2020) and with downslope size sorting on natural talus and scree slopes (Statham, 1976). We examine this

10   topic in the second companion paper (Furbish et al., 2020a); here we offer a synopsis, which centers on the interpretation and significance of the quantities μ and α.

Recall that the formulation is based on the assumption that a change in translational kinetic energy ΔE_p associated with a particle-surface collision can be expressed as $\Delta E_p = -\beta_x E_p$ so that $\beta_x = -\Delta E_p / E_p$ is the proportion of the energy extracted during the collision. Both ΔE_p and β_x are random variables. As described in Appendix E, in general we may write the energy

15   balance of a particle as

$$\Delta E_p = -\Delta E_r - f_c - f_y. \tag{84}$$

Here, a positive change in rotational energy ΔE_r is seen as an extraction of translational energy. This loss of translational energy with the onset of rotation may be relatively large if a collision involves stick following initial sliding due to a large normal impulse, and such a loss also may occur due to the imposed torque of friction during a collision that does not necessarily

20   involve stick. The term f_c in Eq. (84) represents losses associated with particle and surface deformation as well as work performed against friction during collision impulses (thence converted to heat, sound, etc.). But this term also includes losses associated with deformation of the surface at a scale larger than that of an idealized particle-surface impulse contact, namely, due to momentum exchanges associated with the sputtering of loose surface particles during collision. (The videos published as supplementary material to DiBiase et al. (2017) nicely illustrate this sputtering as well as the onset of rotational motion.) The

25   term f_y in Eq. (84) represents the energy loss associated with glancing collisions that produce transverse translational motions and rotation oriented differently than any incident rotation. In some cases the change in energy ΔE_p can be expressed directly in terms of the energy state E_p (Appendix E). However, the complexity of particle-surface collisions on natural hillslopes precludes explicitly demonstrating such a relation for all possible scenarios. Nonetheless, it is entirely defensible to assume that energy losses can be related to the energy state E_p if the elements involved are formally viewed as random variables. Then,

30   the simple relation $\Delta E_p = -\beta_x E_p$ is to be viewed as an hypothesis to be tested against data.

This hypothesis formally enters the formulation via the right side of Eq. (58). Namely, from this relation we may write $\mu \sim \langle \beta_x \rangle$, highlighting that μ is associated with the cooling rate. In turn, particle collision mechanics (Appendix E) suggest, for example, that $\mu \sim \langle \beta_x \rangle \sim M(\theta)$, where $M(\theta)$ involves the coefficients associated with tangential and normal impulses contributing to energy losses during collisions, and depends on the slope angle θ in that the expected surface normal impact

velocity varies with this angle. (In an idealized particle-surface collision these coefficients include the normal coefficient of restitution and a coefficient describing the ratio of tangential to normal impulses during the collision (e.g., Brach, 1991; Brach and Dunn, 1992, 1995)). Moreover, $M(\theta)$ is independent of particle size.

In turn, focusing on the definition of the deposition length scale L_c, Eq. (51), α may be viewed as representing a direct effect of heating described by $mg\sin\theta$, namely, to decrease the likelihood of deposition by decreasing the proportion of particles that cool to sufficiently low energies for deposition to occur — which translates to suppressing the disentrainment rate and increasing the length scale of deposition L_c relative to the cooling length scale $l_c = E_h/mg\mu\cos\theta$. Specifically, heating decreases the spatial rate of the Poisson deposition process below that which would occur in the absence of heating. In this view, μ goes with the cooling rate (not the deposition rate). But we also may write Eq. (51) as in Eq. (53). Viewed in this manner, we may define an apparent friction factor as $\mu_0 = \mu(1-\mu_1 Ki)$ associated with deposition. Here again, μ is associated with the cooling rate but is then modulated by heating. We suggest in the second companion paper (Furbish et al. 2020a) that for the same particle size, α increases with increasing Ki, very likely due to a combination of increased heating and increased partitioning of translational energy to rotational motion (Dorren, 2003; Luckman, 2013) — both decreasing the likelihood of stopping and not represented in just the factor μ. We also suggest that for the same slope and surface roughness, α increases with increasing particle size, decreasing the likelihood of frictional loss with increasing rotation.

Turning to the factor γ (which does not appear in Eq. (83)), recall that an increasing value ($\gamma > 1$) reflects an increasing availability of low energy particles for deposition. Here is what we know. On the one hand, γ cannot be close to unity with randomization of motions by collisional friction, or if the initial downslope energies E_{p0} are not a fixed value. That is, if the distribution of energies $f_{E_p}(E_p, 0)$ has finite variance, then $\gamma > 1$. On the other hand, γ cannot be very large, or deposition would dominate over small distances without long motions that are observed — unless the Kirkby number Ki is unrealistically large. It is possible to qualitatively explore possible values of γ based on assuming different forms of the distribution of energies (and we have done this), but in the absence of knowing the specific form of the distribution, this exercise is not particularly meaningful. In the companion paper we show that fits of experimental travel distances to the theoretical distribution $f_x(x)$ are relatively insensitive to the specific value of γ selected.

5 Related formulations

Here we briefly examine three related formulations of particle disentrainment, focusing on the mechanical basis of this work for comparison with the formulation above. (We examine associated experiments in the companion paper.) We start with the formulations of Kirkby and Statham (1975) and Gabet and Mendoza (2012). These begin with descriptions of particle motions over time rather than space, centered on consideration of a combination of momentum and energy. We then consider elements of the probabilistic formulation presented by Furbish and Haff (2010), Furbish and Roering (2013) and Doane et al. (2018).

5.1 Kirkby-Statham formulation

In their study of particle motions on scree surfaces, Kirkby and Statham (1975) start with a statement of conservation of energy for a particle falling from height h at $x = 0$ onto a rough surface inclined at an angle θ. Namely, if $w_0 = \sqrt{2gh}$ is the vertical impact velocity, then it is assumed that the initial downslope velocity on average is $u_0 = w_0 \sin \theta$. (This actually should be $u_0 = \epsilon w_0 \sin \theta$ with the normal coefficient of restitution ϵ.) The initial downslope particle energy therefore is $(1/2)mu_0^2 = \epsilon^2 mgh \sin^2 \theta = E_{p0}$. In turn, because work is $W = F_x l$, where F_x is the downslope force and l is a displacement, then for a fixed force F_x the displacement is $l = W/F_x$. Assuming that W must be equal to the initial kinetic energy E_{p0} (that is, this initial energy is dissipated over the distance l), then $l = E_{p0}/F_x$. Assuming a Coulomb-like friction behavior, $F_x = mg \sin \theta - \mu_d mg \cos \theta$, where μ_d is a dynamic friction coefficient. Upon asserting that the length l represents the expected travel distance μ_x,

$$\mu_x = -\frac{E_{p0}}{mg \sin \theta - \mu_d mg \cos \theta} = -\frac{\epsilon^2 h \sin^2 \theta}{\sin \theta - \mu_d \cos \theta}, \tag{85}$$

where it is assumed that $|\mu_d \cos \theta| \geq \sin \theta$. As described below, this is equivalent to assuming that particle energy decreases linearly with distance.

This formulation correctly describes the motion of an individual particle that experiences a fixed Coulomb-like friction force, but it cannot represent the rarefied behavior of an ensemble of particles. Nonetheless, it shares elements of the preceding formulation. Namely, in comparing Eq. (85) with Eq. (83), let us momentarily set aside the fact that E_{p0} cannot represent E_{a0} except in the limit of zero variance of initial energy states ($\gamma = 1$), and that the friction factor μ in Eq. (83) and the dynamic friction coefficient μ_d in Eq. (85) have different interpretations. These two descriptions of the average travel distance μ_x then converge in the limit of $\alpha \to \infty$. Inasmuch as Eq. (52) correctly describes the behavior of α, this limit coincides with $Ki \to 1$.

More generally, Eq. (85) implies that the deposition rate is independent of the extant energy state of particles. If Eq. (85) denotes the average of a distribution of travel distances with fixed disentrainment rate, then this fixed rate $P_x = 1/\mu_x$. In dimensionless form this is

$$P_{\hat{x}} = \frac{1 - Ki}{\hat{E}_{p0}}. \tag{86}$$

That is, Eq.(86) cannot allow for the possibility of variations in the cooling rate or heating rate that give spatial variations in the disentrainment rate, as in Eq. (72). The resulting distribution $f_x(x)$ of travel distances therefore is exponential for all $Ki < 1$.

Interestingly, the formulation of Kirkby and Statham (1975) is equivalent to (Appendix I)

$$\frac{\mathrm{d}E_p}{\mathrm{d}x} = mg \sin \theta - mg \mu_d \cos \theta. \tag{87}$$

This is like Eq. (57), but lacks the heating effect of deposition. Like Eq. (85), Eq. (87) implies that deposition is independent of the extant energy state; and when $Ki = 1$ the energy E_p remains fixed as $x \to \infty$ (again noting that E_{p0} cannot represent E_{a0} except in the limit of zero variance of initial energy states).

Dorren (2003) provides a review of efforts to elaborate the Kirky-Statham description of particle motions in relation to hazard assessment. These mostly appeal to a Coulomb-like frictional behavior and are focused on predicting rockfall runout distances.

5.2 Gabet-Mendoza formulation

5 In support of their experimental work involving particle motions on a rough, inclined surface, Gabet and Mendoza (2012) appeal to ideas from Quartier et al. (2000) and Samson et al. (1998) and assume that particle acceleration is described as a linear combination of the gravitational force, a Coulomb-like friction and collisional friction, namely,

$$
\frac{\mathrm{d}u(t)}{\mathrm{d}t} = g\sin\theta - \mu_d g\cos\theta - \kappa u^\psi . \tag{88}
$$

As written, the dimensions of the coefficient κ depend on the value of the exponent ψ, which is thought to vary between one
10 and two based on experiments. The principal significance of this formulation is that it points to the idea of collisional friction, thus representing an important step beyond the Coulomb-like model of Kirkby and Statham (1975). However, because there is confusion in the literature regarding the form and interpretation of Eq. (88), we summarize the basis of this formulation in Appendix J. The essence is this: The Coulomb term and the collisional term as written are not additive for an individual particle. The collisional term is a stochastic quantity and applies to an averaged behavior, not to the instantaneous behavior
15 of an individual particle. If this term is involved, the velocity u must be considered a time-averaged or ensemble-averaged velocity, or Eq. (88) must be recast as a Langevin-like equation. Parts of this formulation are appropriate for describing the behavior of particles that roll bumpety-bump over a surface roughened with a monolayer of particles, but this formulation is problematic in its description of the mechanics involved in rarefied motions over the roughness of natural hillslopes.

In both formulations above the idea of a Coulomb-like friction with a dynamic friction coefficient is mechanically unsound
20 (Appendix J). For particles that tumble, bounce and skitter down a rough surface, the static normal weight of a particle, $mg\cos\theta$, does not set the particle-surface friction. Rather, dynamic forces during collision impulses matter (Brach, 1991; Stronge, 2000). This includes the dynamic Coulomb-like friction force associated with conversion of translational to rotational kinetic energy during collisions (Appendix E). Formulating a dynamic friction coefficient would require ensemble averaging of the ratio of tangential to normal momentum exchanges, both of which are random variables. A Coulomb-like friction is
25 appropriate for solid body and dense granular motions, but not for the rarefied conditions described here.

5.3 Furbish-Haff-Roering-Doane formulation

The probabilistic formulation presented by Furbish and Haff (2010), Furbish and Roering (2013) and Doane et al. (2018) assumes that travel distances are described by an exponential distribution whose mean μ_x is a function of the local slope S. Namely, the mean increases with S and becomes unbounded as S approaches a critical value S_c. This formulation is equivalent
30 to setting the mean $\mu_x \sim L_c$. Here we consider the behavior of L_c over small S then as $S \to S_c$.

Starting with Eq. (49) we write

$$L_c \sim \frac{\alpha E_h}{mg\mu\cos\theta} = \frac{\alpha E_h}{mg\mu}\sqrt{1+S^2}. \tag{89}$$

If α is described by Eq. (52), and neglecting the factor μ_1 for simplicity, then this is

$$L_c \sim= \frac{\alpha_0 E_h}{mg\mu}\frac{\sqrt{1+S^2}}{1-Ki} = \frac{\alpha_0 E_h}{mg\mu}\frac{\sqrt{1+S^2}}{1-S/\mu}. \tag{90}$$

A binomial expansion of Eq. (89) gives

$$L_c \sim \frac{\alpha E_h}{mg\mu}\left(1+\frac{S^2}{2}+...\right), \tag{91}$$

and Eq. (90) gives

$$L_c \sim \frac{\alpha_0 E_h}{mg\mu}\left(1+\frac{S^2}{2}+...\right)\left(1+\frac{S}{\mu}+...\right)$$

$$= \frac{\alpha_0 E_h}{mg\mu}\left(1+\frac{S}{\mu}+\frac{S^2}{2}+...\right). \tag{92}$$

From Furbish and Haff (2010),

$$L_c \sim \lambda_0\left(\frac{S_c+S}{S_c-S}\right) = \lambda_0\left(1+\frac{2S}{S_c}+\frac{S^2}{S_c^2}+...\right). \tag{93}$$

If we interpret the length scale $\lambda_0 \sim \alpha E_h/mg\mu$, then for small to modest slopes S, Eq. (91) and Eq. (93) differ in their linear versus quadratic forms at lowest order. If $\lambda \sim \alpha_0 E_h/mg\mu$, then the behavior of Eq. (92) and Eq. (93) are the same if $S_c = 2\mu$. More generally, Eq. (92) and Eq. (93) display the same behavior with increasing S. Namely, if the critical slope is interpreted as $S_c \sim \mu$, the length scale L_c in both cases increases approximately linearly over much of the domain of S then asymptotically becomes unbounded as $S \rightarrow S_c$.

Note that the formulation involving Eq. (93) is limited to an exponential form of the distribution of travel distances (Furbish and Haff, 2010; Furbish and Roering, 2013; Doane et al., 2018). It does not mimic the different forms of $f_x(x)$ illustrated in Figure 4, and it lacks a mechanical underpinning as presented in previous sections.

6 Varying disentrainment rate

The formulations above envision particle motions starting at position $x = 0$ such that the distribution of travel distances is expressed as $f_x(x)$. This is particularly convenient when considering laboratory and field experiments in which particles are released on a sloping surface from the same starting position, as examined in the companion paper. Here we return to our starting point concerning calculations of the particle flux and use of the entrainment form of the Exner equation as summarized in Section 2. Recall that in this frame of reference the particle travel distance is denoted by r and the starting position may

involve any position x. Then, with reference to Eq. (4), Eq. (5) and Eq. (6), the disentrainment rate is $P_r(r;x)$, the distribution of travel distances r is $f_r(r;x)$ and the exceedance probability (survival function) is $R_r(r;x) = 1 - F_r(r;x)$. In turn, for particles starting at x, the mean travel distance is $\mu_r(x)$.

To use the results of Section 2.1 in specifying the exceedance probability $R_r(r;x)$ and the probability density $f_r(r;x)$ in the

5 entrainment forms of the flux and the Exner equation, Eq. (5) and Eq. (6), requires a key assumption. Namely, one must assume that the factors controlling the disentrainment rate on a hillslope change sufficiently slowly over x such that these factors defined at any position x correctly determine the conditions for the downslope motions of particles starting at x (Furbish and Roering, 2013; Doane et al., 2018). This is equivalent to assuming that during its downslope motion a particle "sees" conditions similar to those at its starting position. However, in actuality particles may see new conditions during their motions that change their

10 behavior relative to what was "predicted" by the conditions at their starting positions. Let λ_S denote a characteristic distance over which conditions persist. For example, focusing on the Kirky number Ki,

$$\lambda_S \sim \frac{Ki}{\partial Ki/\partial x} \,. \tag{94}$$

Thus, a rapid change in Ki over position x implies that λ_S is small, and if Ki changes slowly then λ_S is large. Uniform conditions imply that $\lambda_S \to \infty$. We may then assume that if $\mu_x \ll \lambda_S$, conditions change sufficiently slowly that use of the

15 continuous forms of $R_r(r;x)$ and $f_r(r;x)$ with Eq. (5) and Eq. (6) provides a reasonable approximation of collective particle behavior.

This strategy might be acceptable for an exponential-like distribution with finite moments, but it is problematic if particle travel distances r involve a heavy-tailed distribution or if conditions transition along x between net cooling and net heating, or vice versa. Herein resides the merit of the discrete form of the disentrainment rate and the distribution of travel distribution

20 as summarized in Section 2.2. Recall that this formulation is aimed at describing the ingredients of disentrainment that are occurring at different locations on a hillslope, where the mechanical behavior at a location transitions to another behavior in the downslope direction. In this formulation we let p_k denote the probability that a particle, having not been disentrained before the kth interval, then becomes disentrained within this interval.

Let $\mathrm{d}r$ denote a finite (rather than infinitesimal) interval. Then the kth interval begins at r and ends at $r + \mathrm{d}r$. Letting

25 $N_k = N(r)$ denote the number of particles reaching the kth interval, then based on Eq. (56) the probability that a particle will be disentrained within this interval is

$$p_k = -\frac{1}{N_k}\mathrm{d}N = \frac{\gamma}{\alpha} mg\mu \cos\theta \frac{1}{E_a}\,\mathrm{d}r \tag{95}$$

This will be recognized as the setup for a simple finite-difference scheme, to be coupled with a similar finite-difference expression for the average energy state E_a. Namely, in dimensionless form, for particles starting at position $\hat{x}$,

30 $$\hat{N}(\hat{r} + \mathrm{d}\hat{r}; \hat{x}) \approx \hat{N}(\hat{r}; \hat{x}) - \frac{\gamma}{\alpha} \frac{\hat{N}(\hat{r}; \hat{x})}{\hat{E}_a(\hat{r}; \hat{x})}\,\mathrm{d}\hat{r} \quad \text{and} \tag{96}$$

$$\hat{E}_a(\hat{r} + \mathrm{d}\hat{r}; \hat{x}) \approx \hat{E}_a(\hat{r}; \hat{x}) + \left(Ki - 1 + \frac{\gamma}{\alpha} - \frac{1}{\alpha} \right)(\hat{r}; \hat{x})\,\mathrm{d}\hat{r}$$

$$= \hat{E}_a(\hat{r}; \hat{x}) + [Ki(\hat{r}; \hat{x}) - Ki_*(\hat{r}; \hat{x})] \, d\hat{r}, \tag{97}$$

where both the Kirky number Ki and the elements of the transition value of the Kirkby number $Ki_* = 1 - \gamma/\alpha + 1/\alpha$ may vary from one interval to the next as conditions vary in the downslope direction. The proportion of $\hat{N}(0; \hat{x})$ particles starting from position $\hat{x}$ is then recovered from

$$f_k(k; \hat{x}) \approx -\frac{1}{\hat{N}(0; \hat{x})} [\hat{N}(\hat{r} + d\hat{r}; \hat{x}) - \hat{N}(\hat{r}; \hat{x})]$$

$$= -\frac{1}{\hat{N}(0; \hat{x})} [\hat{N}(k+1; \hat{x}) - \hat{N}(k; \hat{x})]. \tag{98}$$

We note that, although different in form and implementation, this description is similar to the particle-based scheme of Tucker and Bradley (2010) in which particle behavior adjusts to newly encountered conditions during downslope motion.

Consider for illustration a situation in which the Kirkby numbers Ki and Ki_* systematically vary with position $\hat{x}$, relative to uniform conditions (Figure 5). This may be due, for example, to variations in steepness or in the friction μ with increasing
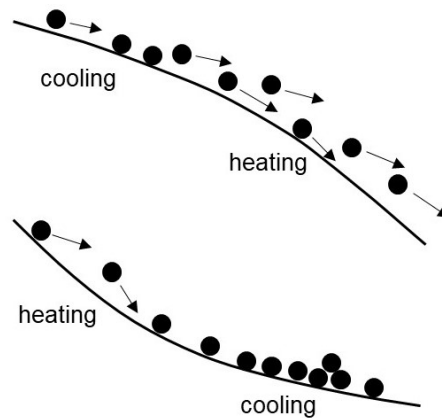
Figure 5. Cartoon of hillslope surfaces with downslope variations in steepness leading to concomitant variations in heating, cooling and deposition; this is in contrast to a planar slope with uniform μ that produces either net heating or net cooling, or isothermal conditions.

travel distance. Also recall that $Ki < Ki_*$ implies cooling whereas $Ki > Ki_*$ implies heating.

In these examples we let α vary with the Kirkby number Ki according to Eq. (52) in anticipation of results presented in the companion paper. A decreasing rate of cooling associated with, for example, steepening in the downslope direction generally increases the heaviness of the tail of the distribution relative to the tail associated with a fixed rate of cooling (Figure 6). We present evidence in the companion paper that this occurs in the field-based experiments reported by DiBiase et al. (2017). Specifically, particles were launched down a rough hillslope surface, and then their travel distances were measured over a 14
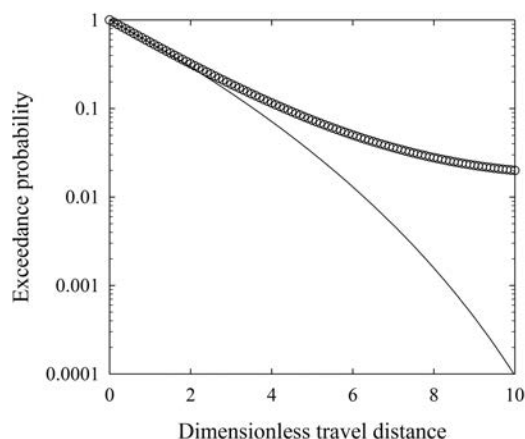
Figure 6. Plot of exceedance probability $R_{\hat{x}}(\hat{x})$ versus dimensionless travel distance $\hat{x}$ showing conditions with fixed net cooling (solid line) and conditions that start with the same cooling rate but then involve a decreasing rate with increasing distance $\hat{x}$ (circles). In this example the Kirkby number starts at $Ki = 0.70$ at $\hat{x} = 0$ and increases to $Ki = 0.96$ at $\hat{x} = 10$.

m interval. Particles reaching the steeper slope below the measurement interval continued to the base of the hillslope without stopping. In turn, an increasing rate of cooling (e.g., with decreasing slope in the downslope direction) generally lightens the tail, and may lead to truncation of the distribution if the rate increases rapidly enough. Moreover, a condition involving initial heating followed by cooling (e.g., with a concave hillslope surface) can lead to a distribution with a finite mode (Figure 7). These examples represent situations where particle travel distances cannot necessarily be approximated by a distribution whose
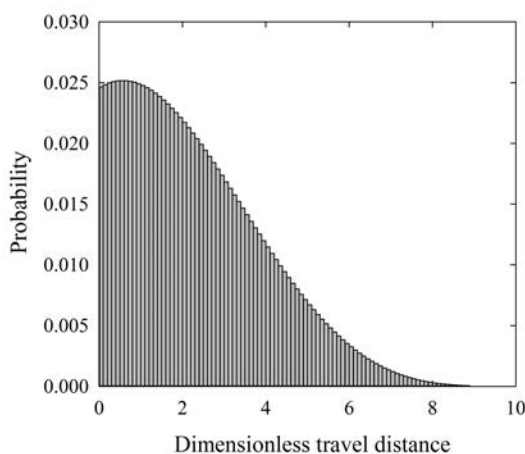
Figure 7. Probability mass function $f_k(k; \hat{x})$ of discrete travel distances k associated with initial net heating over small k followed by net cooling with increasing k, leading to a finite mode. In this example the Kirkby number starts at $Ki = 0.90$ at $k d\hat{r} = \hat{x} = 0$ and decreases to $Ki = 0.57$ at $k d\hat{r} = \hat{x} = 10$.

5

parametric values are set by the hillslope conditions at the position where particle motions start. We defer further examination
of this behavior, including use of the convolutions in Eq. (5) and Eq. (6), for a later time.

7 Discussion and conclusions

Our formulation of rarefied particle motions is based on a description of the energy balance of a cohort of particles treated
5 as a rarefied granular gas, and a description of particle deposition that depends on the energy state of the particles. The
formulation leads to a generalized Pareto distribution of particle travel distances, Eq. (74). This distribution represents three
well-defined behaviors in which the Kirkby number Ki — the ratio of graviational heating to frictional cooling — has a
principal role. Conditions with relatively small Ki lead to rapid thermal collapse such that the distribution of travel distances
is bounded. For intermediate values of Ki the rate of gravitational heating may be matched by the rate of frictional cooling,
10 giving approximately isothermal conditions and an exponential distribution of travel distances. Conditions with large Ki and
net heating lead to a heavy-tailed distribution of travel distances. We provide compelling evidence of all three behaviors in our
companion paper (Furbish et al., 2020a). Here we emphasize that we do not choose the generalized Pareto distribution in the
empirical manner of selecting a distribution based on goodness-of-fit criteria applied to data sets. Rather, this distribution is
dictated by the physics of the problem, just as, for example, the Boltzmann distribution (an exponential distribution) emerges
15 in classical statistical mechanics from consideration of the accessible energy microstates of a gas system. We elaborate this
point in the third companion paper (Furbish et al., 2020b).

   Two of the most important elements of the formulation are the deposition length scales $l_c(E_p)$ and $L_c(E_h)$, the former being
keyed to the specific particle energy state E_p and the latter being keyed to the harmonic average energy E_h of the particle
cohort. Indeed, these lengths provide the essential connection between particle deposition and the energy balance of the particle
20 cohort. We assume that l_c is set by the advective cooling length scale in the Fokker-Planck equation, that is, Eq. (44). This is
a natural choice in that deposition must go with cooling. The energy specific deposition rate in the absence of heating is then
specified as if deposition proceeds as a spatial Poisson process. We emphasize that this represents a maximum (information)
entropy choice in the sense that it is faithful to what we think we know, namely, the connection between deposition and cooling,
as well as to what we do not know (Jaynes, 1957a, 1957b), namely, any detailed physics that would produce a different rate
25 (for example, involving a nonlinear dependence on energy state) but which cannot be specified or constrained with available
information. This description then leads to the interesting result, Eq. (46), that the loss of total energy due to deposition appears
to be independent of the energy state. In particular, the loss of large energy states occurs at a relatively slow rate whereas the
loss of small energy states occurs at a relatively fast rate. In effect the rate of loss of energy per energy interval is fixed across
energy states. The result is that the energy E_p cancels with substitution of Eq. (45) into the integral in Eq. (46) such that the
30 total loss becomes independent of the energy state. That is, the loss of total energy goes simply with the loss of particles (and
the energy they possess).

   In turn, the total deposition rate is energy dependent. This rate, defined by the length scale L_c, is obtained by integrating
the number density of particles over all possible energy states as in Eq. (48). Because l_c is keyed to the energy state E_p,

but the integral in Eq. (48) does not involve this energy in the numerator, the result involves the reciprocal of the harmonic average energy E_h. In general, the harmonic average diverges from the arithmetic average E_a with increasing variance of the distribution of energy states. With $E_a/E_a = \gamma$, the resulting ratio γ/E_a in Eq. (56) (with dimensionless form given by Eq. (61) or Eq. (64)) reflects an increasing proportion of lower energy particles available for deposition, relative to this availability

5   with $\gamma \to 1$. This effect is directly apparent in the expression of the mean travel distance, Eq. (69), associated with isothermal conditions.

Note that the formulation does not involve specifying a threshold energy for deposition. Such an idea is mechanically irrelevant. Whereas low energy particles are on average more likely to become disentrained than are high energy particles, a set of particles with precisely the same low energy will for probabilistic reasons not be disentrained simultaneously. Each particle

10   experiences a unique set of conditions that disentrain it; and because of this uniqueness of conditions a particle with energy below an arbitrarily assigned threshold can with finite probability be gravitationally reheated to a higher energy state. For given particle and surface roughness conditions, the formulation treats this aspect of disentrainment as a probabilistic process. In effect, this aspect is incorporated into the deposition lengths l_c and L_c as these are related to the distribution of particle energy states and the probabilistically expected extraction of energy during collisions.

15   Frictional cooling is formulated in terms of extraction of translational kinetic energy associated with particle-surface collisions. This involves the random variable $\beta_x = -\Delta E_p/E_p$ whose energy specific average $\overline{\beta_x}$ is the expected proportion of energy extracted from particles with energy E_p. In detail the change in energy ΔE_p may be partitioned between a frictional loss, any conversion of translational to rotational energy, and any apparent loss associated with downslope incident motion reflected to transverse motion during a glancing collision. Our treatment of β_x as a random variable does not distinguish the

20   details involved in collisions. Yet these details may be important in terms of effects of different particle sizes and shapes, specifically the likelihood that the partitioning of energy losses differs between sizes or shapes. Herein the quantity α has a dualistic role. As incorporated in Eq. (51), this quantity represents the effect of heating, namely, to decrease the likelihood of deposition by decreasing the proportion of particles that cool to sufficiently low energies for deposition to occur — which translates to suppressing the disentrainment rate and increasing the length scale of deposition L_c. As incorporated in Eq. (53),

25   this quantity modulates the frictional cooling described by $\mu \propto \langle \beta_x \rangle$ to give an apparent decrease in friction associated with deposition.

Whereas particles that are small relative to the surface roughness texture are on average more likely to experience near collinear collisions with surface bumps and be "captured" within divots and pockets, particles that are large relative to the roughness texture are less likely to experience direct collisions with, or strong deflections by, smaller surface bumps. In ad-

30   dition, large particles are more likely to experience conversion of their translational energy into rotational energy with less loss during collisions. In particular, large spherical particles are more likely to roll or spin with increased heating, and large spinning particles are less likely than are smaller particles to be frictionally cooled. These points are reflected in the laboratory experiments of Samson et al. (1998, 1999) (Appendix J), the laboratory experiments of Kirkby and Statham (1975) and the field experiments of DiBiase et al. (2017) and Roth et al. (2020) (see the second companion paper (Furbish et al., 2020a)). This

35   also implies that for a given slope angle and surface roughness, some particle sizes may experience net cooling while some

sizes experience net heating (Roth et al., 2020), likely contributing to the size sorting observed on many talus and scree slopes (Kirkby and Statham, 1975; Statham, 1976; Luckman, 2013). We suspect the noticeable sorting in Figure 1 is due to these effects.

The formulation readily accommodates the idea of a mixed distribution composed of different distributions associated with different particle sizes or mechanical behaviors. This amounts to forming a sum of distributions, each weighted in proportion to the size classes involved in transport. As with individual sizes, the formulation assumes rarefied conditions — that particles of different sizes do not interact during their downslope motions, or that such interactions negligibly influence the particle energy balance relative to particle-surface interactions. We provide an example in the second companion paper (Furbish et al., 2020a).

With rockfall and subsequent particle motions over talus and scree surfaces, the initial energy state E_{a0} can be approximated in terms of the fall height (Kirkby and Statham, 1975). But this is a special situation in which the initial energy can be reasonably constrained. More generally, and with reference to the entrainment forms of the flux and the Exner equation, Eq. (5) and Eq. (6), we are concerned with entrainment of particles from many if not all positions on a hillslope in relation to disturbances. This points to the idea that entrainment, if followed by long distance motions, requires sufficient initial heating to keep particles moving downslope. This in turn echoes the conclusion of Doane et al. (2018a), that correctly specifying the entrainment rate is a key part of implementing formulations of nonlocal transport and mass conservation. Because of the significance of sediment capacitors (e.g., vegetation) in trapping and storing sediment on hillslopes (Lamb et al., 2013; Doane, 2018a), there is merit in clarifying the initial energetics of particles upon their release (i.e., entrainment) from storage. There also is a need to examine re-entrainment and transport associated with particle collisions, analogous to work on particle splash during aeolian transport and the energetics of collective entrainment (Ancey et al., 2008) by collisions during bed load transport (Lee and Jerolmack, 2018).

That the energy and mass balances are expressed in the form of coupled differential equations opens the possibility of describing effects of varying disentrainment rates in response to changing downslope conditions in a manner intrinsic to particle-based treatments of transport (Tucker and Bradley, 2010), but not readily incorporated in previous probabilistic descriptions. Namely, if surface conditions change in the downslope direction, for example, giving net cooling followed by heating or vice versa (Figure 5), then particles whose travel distances are large enough "see" this change and their behavior concomitantly changes. In this case the coupled equations of energy and mass in principle can be solved to accommodate these changing conditions. Interestingly, as differential (or finite difference) equations these have a local form, yet they intrinsically represent nonlocal behavior in that information concerning the energy state E_a and the mass N is cumulatively handed from one position to the next downslope. In turn, the forms of $R_r(r; x')$ and $f_r(r; x')$ associated with any position x' in the expressions of the flux and its divergence, Eq. (5) and Eq. (6), must be based on information downslope from this position.

In this regard, here we offer further perspective on what is meant by local versus nonlocal transport on hillslopes. A transition of travel distances involving a distribution with a light tail to one with a heavy tail, as embodied in the generalized Pareto distribution, does not distinguish local from nonlocal transport. As fully explained in Furbish and Roering (2013) and in Furbish et al. (2016), the convolutions in Eq. (5) and Eq. (6) represent nonlocal transport regardless of the form of the probability density function $f_r(r; x)$ and its associated exceedance probability function $R_r(r; x)$. These scale independent expressions are

just specialized forms of the Master equation used in probabilistic descriptions of particle motions over a remarkable range of scales (Einstein, 1905; von Smoluchowski, 1906; Chandrasekhar, 1943 Risken, 1984). Nonlocal transport is a physical thing, and refers to the idea that attributes of particle motions used in defining the rheology, the flux or its divergence at a position x depend on conditions "far" from this position (e.g., Bocquet et al., 2009; Brantov and Bychenkov, 2013; Henann

5 and Kamrin, 2013). In contrast, local transport is a mathematical thing, not a physical thing, and refers to the idea that under certain circumstances the convolution form of the Master equation can be approximated such that the flux or its divergence has the form of a local mathematical expression — for example, a Fokker-Planck equation — whose terms involve conditions associated with the local position x. As alluded to above, a local expression can be formulated when the distribution $f_r(r; x)$ has finite moments and is peaked near the origin ($r = 0$). A heavy-tailed behavior means that this is not justified. Rather, the

10 full convolution or a fractional derivative approximation of it must be used (Schumer et al., 2009). Because of the generality and scale independence embodied in the Master equation and the convolutions in Eq. (5) and Eq. (6), the use of "nonlocal" as a qualifier of "transport" in reference to hillslopes actually is redundant (Doane, 2018). Its use is merely a reminder that the flux or its divergence at a position x depends on things happening upslope.

The entrainment rate $E_s(x)$, the exceedance probability function $R(r; x)$ and the distribution of travel distances $f_r(r; x)$

15 within the integrals in Eq. (5) and Eq. (6) are treated as continuous functions. However, this does not imply a continuum behavior. Like the Fokker-Planck equation, which describes the evolution of the probability density function of a random variable that may or may not satisfy the continuum hypothesis (see Appendix A in Furbish et al., 2018b), the continuous forms of Eq. (5) and Eq. (6) represent a probabilistic description of expected behavior, not necessarily the behavior of any one realization (system). In practical terms, imagine a rockfall event from a cliff face involving an individual particle or a relatively

20 small number of particles whose subsequent downslope motions then start at position $x = 0$ at the base of the cliff. Inasmuch as the generalized Pareto distribution $f_x(x)$ provides the correct description of the expected behavior of the particles from the rockfall event, then these particles may be viewed as a (small) sample drawn from this distribution. The outcome of each realization (sample) is almost certainly different from all other realizations. Over a period of time the pooled outcomes (travel distances) of many events converge to the smooth representations given by $f_x(x)$ and $R_x(x)$ — as if Gabet and Mendoza

25 (2012), DiBiase et al. (2017) and Roth et al. (2020) had performed a gazillion additional rock-launching experiments (see second companion paper, Furbish et al. (2020a)) then pooled the outcomes of these experiments. Implications of this idea are examined further in Furbish and Haff (2010), Furbish and Roering (2013) and Furbish et al. (2016, 2017, 2018b).

The formulation may have interesting implications for examining Martian landforms. For example, the appearance of the acceleration g in Eq. (51), Eq. (56) and Eq. (83) immediately suggests the possibility that particle travel distances are on

30 average significantly longer on Mars than on Earth for otherwise similar particle sizes and surface-roughness conditions; and we are confident in suggesting that future Martians likely will have far more fun than Earthlings in the sport of boulder rolling, notably on the crater rim of Olympus Mons. Nonetheless, we leave it to folks more familiar with Mars than we are to examine this. A key element of doing this is to either assume that the friction factor μ is similar to what occurs on Earth (which may be entirely reasonable) or further unfold the elements of this factor. We comment on this idea again in the second companion

35 paper (Furbish et al., 2020a). We meanwhile note that a similar question arises in relation to the role of g in setting the friction

of granular slopes on Mars. Atwood-Stone and McEwen (2013) address this question by examining dune slip-face angles on Mars, and suggest that the similarity of these angles with those observed on Earth weakens any argument for different granular behavior associated with g — consistent with independent assessments (Moore et al., 1987; Tesson et al., 2020) and the idea that this angle is set by the static granular force-chain network (Cates et al., 1998; Furbish et al., 2008).

5 Appendix A: Choice of terminology

The study of granular materials is concerned with the behavior of the phases of these materials and associated phase transitions (Jaeger et al., 1996; Baldassarri et al., 2005; Daniels and Behringer, 2006; Forterre and Pouliquen, 2008; Jerolmack and Daniels, 2019). These phases and transitions share attributes with ordinary materials — solids, liquids and gases — although granular materials often exhibit behavior that is much different than ordinary materials. Nonetheless, it has become customary in the study of granular materials to adopt terminology similar to that used to describe ordinary materials.

The ideas of heating and cooling of a granular material are straightforward, to mean a change in the granular temperature of the material, specifically the average translational kinetic energy of the particles (but see van Zon and MacKintosh (2004) and Baldassarri et al. (2005)). However, granular materials do not possess an internal energy in the sense that we attribute to the particles of an ordinary liquid or gas. This means that heating of a granular material requires a mechanical input of energy, whereas cooling is associated with dissipative (non-conservative) collisions of particles with each other and with boundaries. In the problem at hand, gravitational heating occurs as particles move downslope, and their gravitational potential energy is converted to kinetic energy. Frictional cooling is associated with dissipative particle-surface interactions (e.g., collisions).

The ideas of melting and freezing of a granular material (Daniels and Behringer, 2006) pertain to the transition between a solid-like phase and a hydrodynamic (fluid-like) phase. However, in the problem at hand, we are concerned with rarefied particle conditions in which disentrainment from the rarefied state to the solid-like state or vice versa does not involve an intermediate hydrodynamic phase (e.g., Haff, 1983; Jenkins and Savage, 1983; Jaeger et al., 1996). Entrainment is akin to sublimation, and disentrainment is akin to deposition (or desublimation). Phase transitions involving an intermediate hydrodynamic phase (evaporation/condensation and melting/freezing) are represented in Earth-surface processes, for example, by melting (entrainment) and freezing (disentrainment) at the base of a granular flow, dry or wet. We recommend the papers by Forterre and Pouliquen (2008), Frey and Church (2011), Houssais et al. (2015) and Jerolmack and Daniels (2019) for perspectives on this emerging topic, notably in relation to transport by shear flows.

Appendix B: Particle cohort

In order to clarify the idea of a cohort of particles associated with a control volume with edge length $\mathrm{d}x$ (Figure 2), here we offer a straightforward thought experiment. As a point of reference, the study of granular gases typically involves consideration of the behavior of an individual system composed of many particles that are mechanically heated, where energy dissipation is associated with particle-particle collisions. In contrast, our problem involves an unusual situation in that we must start by

considering a system composed of one particle, where energy dissipation occurs with particle-surface collisions, and then in turn consider the behavior of an ensemble of such systems.

Imagine a box containing one particle. We mechanically shake the box and the particle is heated. At any instant the particle has kinetic energy E_p. Each time the particle collides with the floor of the box it is re-heated, and each time it collides with a

5 wall of the box energy is extracted. Eventually the particle by chance has sufficiently low energy that when it next encounters a wall it becomes irreversibly deposited (disentrained) onto the wall. Then the box has no moving particle.

Like Gibbs (1902), we now imagine a great number N of nominally identical but independent single-particle systems, where each particle in each system (box) behaves according to the same laws of physics, each undergoing heating and collisional cooling, and occasionally being deposited (Figure B1). We now choose one instant in time and examine the state of each
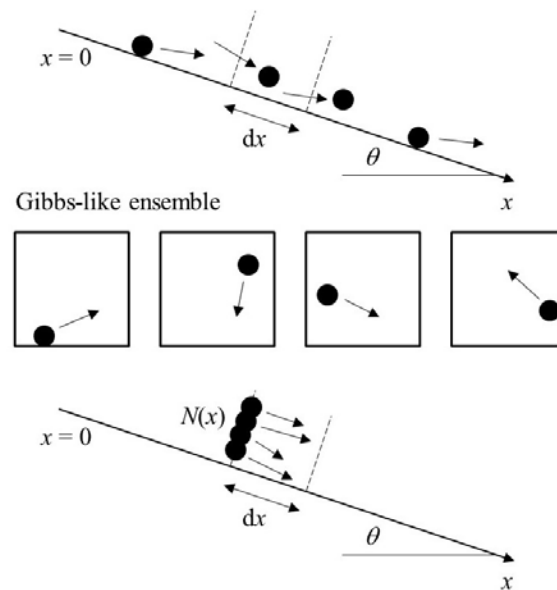
Figure B1. Schematic diagram of surface inclined at angle θ and control volume with edge length $\mathrm{d}x$ through which particles move, with Gibbs-like ensemble of single-particle systems leading to definition of the cohort of $N(x)$ particles starting at the left face of the control volume.

10 particle. Some particles previously have been deposited, so at this instant N refers to those systems whose particles are in motion. At this instant each particle has kinetic energy E_p, and we may define the ensemble probability density $f_{E_p}(E_p)$ of energy states E_p. As a consequence we also may at this instant define the ensemble averaged kinetic energy $\langle E_p \rangle$ and the total energy $E = N\langle E_p \rangle$. (Alternatively, we could imagine all N particles in a single box at one instant, but with the caveat that we must imagine them as not interacting with each other, only with the floor and walls of the box.) We now choose a successive

15 instant in time, namely, $t + \mathrm{d}t$. During $\mathrm{d}t$ the number N has decreased with deposition of some particles, the distribution $f_{E_p}(E_p)$ has changed, and the average energy $\langle E_p \rangle$ and the total energy E have changed.

More generally we can choose N different instants in time t, one instant for each box, and examine the state of each particle. Then, upon collecting the particles as a cohort independently of the selected times, like above we observe an ensemble distribution of energy states with specific average energy $\langle E_p \rangle$ and total energy E. At this point we relax the idea of a box, and simply view particle-wall collisions more generally as particle-surface collisions during motions parallel to x; and instead

5   of heating the particles via particle-floor collisions we imagine this to occur continuously by gravitational heating. We then let the N selected instants in time coincide with those instants that each of the particles is located at a specified position x. That is, these are the $N(x)$ particles located at the left face of the interval x to $x + \mathrm{d}x$ (Figure B1). We may then examine how the number $N(x)$ and the ensemble distribution $f_{E_p}(E_p, x)$ and its moments change over the interval x to $x + \mathrm{d}x$ as this particle cohort moves downslope. Note that each member of the cohort not deposited within this interval may arrive at position

10   $x + \mathrm{d}x$ at a different instant in time. This is unimportant, however, as we are interested only in how the energy states of the particles vary with position x. Similarly, upon choosing any subsequent downslope position x, we must recognize that the $N(x)$ particles reaching this position do so at entirely different instants in time. Here is a final note: In this problem a particle ensemble average is identical to a Gibbs ensemble average.

Appendix C: The Fokker-Planck-like equation

15   Let $q = E_p(x + \mathrm{d}x) - E_p(x)$ denote a change in the energy of a particle over the small distance $\mathrm{d}x$, and let $f_q(q; E_p, x)$ denote the probability density function of the changes q associated with the energy state E_p and position x. If $n_{E_p}(E_p, x)$ denotes the number density of particle energies E_p, then according to the Master equation,

$$n_{E_p}(E_p, x + \mathrm{d}x) =$$

20   $$\int_0^\infty f_q(q; E_p - q, x) n_{E_p}(E_p - q, x) \, \mathrm{d}q. \tag{C1}$$

Assuming the density $f_q(q; E_p, x)$ is peaked near $q = 0$ with finite first and second moments, we may expand the integrand in Eq. (C1) as a Taylor series to second order, subtract $n_{E_p}(E_p, x)$ from both sides, then divide by $\mathrm{d}x$ and take the limit as $\mathrm{d}x \to 0$ to obtain a Fokker-Planck-like equation, namely,

$$\frac{\partial n_{E_p}(E_p, x)}{\partial x} = -\frac{\partial}{\partial E_p}[k_1(E_p, x) n_{E_p}(E_p, x)]$$

25

$$+\frac{1}{2}\frac{\partial^2}{\partial E_p^2}[k_{2c}(E_p, x) n_{E_p}(E_p, x)]. \tag{C2}$$

Here, $k_1(E_p, x)$ is a drift speed and $k_{2c}(E_p, x)$ is a diffusion coefficient defined by

$$k_1(E_p, x) = \lim_{\mathrm{d}x \to 0} \frac{1}{\mathrm{d}x} \int_{-\infty}^\infty q f_q(q; E_p, x) \, \mathrm{d}q \tag{C3}$$

and

$$k_{2c}(E_p, x) = \lim_{dx \to 0} \frac{1}{dx} \int_{-\infty}^{\infty} q^2 f_q(q; E_p, x) \, dE_p. \tag{C4}$$

The drift speed $k_1(E_p, x)$ has two parts, one associated with gravitational heating and one associated with frictional cooling. Starting with gravitational heating, let $h(x)$ denote the height of a particle within the gravitational field at position x. If $E_p(x)$ denotes the particle kinetic energy equal in magnitude to the potential energy $mgh(x)$ at height $h(x)$, then $E_p(x + dx) = mgh(x + dx)$ is the magnitude of the particle kinetic energy at the height $h(x + dx)$, assuming a complete conversion of gravitational to kinetic energy without loss. Thus,

$$q = mg[h(x + dx) - h(x)]. \tag{C5}$$

This indicates that q in Eq. (C3) is independent of the energy state E_p and therefore may be removed from the integral. We thus write Eq. (C3) as

$$k_{1h} = mg \lim_{dx \to 0} \frac{h(x + dx) - h(x)}{dx} \int_{-\infty}^{\infty} f_q(q; E_p, x) \, dq$$

$$= mg \frac{dh}{dx} = mg \sin \theta. \tag{C6}$$

This is the steady rate of gravitational heating.

The part of $k_1(E_p, x)$ associated with frictional cooling is obtained as follows. With particle-surface collisions we may assume that q is proportional to the expected value of ΔE_p. In turn we let $n_x = 1/\lambda$ denote the expected number of collisions per unit distance, where λ is the expected travel distance between collisions. This leads to

$$k_{1c}(E_p, x) = \frac{d\overline{q}}{dx} \approx n_x \overline{\Delta E_p} = n_x \overline{\beta_x} E_p, \tag{C7}$$

where the overline denotes an average over particles at the energy state E_p (rather than a global average).

Because gravitational heating is a fixed quantity according to Eq. (C6), heating does not involve diffusion. In turn, the diffusion coefficient $k_{2c}(E_p, x)$ associated with frictional cooling is given by

$$k_{2c}(E_p, x) = \frac{d\overline{q^2}}{dx} \approx n_x \overline{(\Delta E_p)^2} = n_x \overline{\beta_x^2} E_p^2. \tag{C8}$$

Note that whereas k_{1h} is a fixed quantity, k_{1c} and k_{2c} must be viewed as statistically expected quantities.

Appendix D: Expected travel distance between collisions

Momentarily let $v = \langle u^2 \rangle^{1/2}$, and then let v_0 denote the surface-parallel velocity of a particle rebounding with reflection angle ϕ measured from the surface (Figure D1). We then know that

$$U_0 = v_0 \frac{\cos(\phi - \theta)}{\cos \phi} \quad \text{and} \quad W_0 = v_0 \frac{\sin(\phi - \theta)}{\cos \phi}, \tag{D1}$$
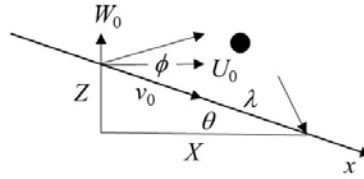
Figure D1. Definition diagram for determining travel distance λ.

where U_0 denotes the horizontal velocity and W_0 denotes the vertical velocity. For a vertical change in elevation Z over a horizontal distance X associated with the surface-parallel distance λ, we know that $Z = -SX = -SU_0 t_0$, where t_0 is the travel time. For a rebounding particle starting at position $z_0 = 0$ we may deduce from Newton's second law that

$$Z = -SU_0 t_0 = -\frac{1}{2} g t_0^2 + W_0 t_0, \tag{D2}$$

5   which gives

$$t_0 = \frac{2W_0}{g} + \frac{2SU_0}{g}. \tag{D3}$$

With $\lambda = X/\cos\theta = U_0 t_0/\cos\theta$, we then combine Eq. (D1), Eq. (D2) and Eq. (D3) to obtain

$$\lambda = \frac{2v_0^2 \sin(\phi-\theta)\cos(\phi-\theta)}{g\cos^2\phi\cos\theta} + \frac{2Sv_0^2\cos^2(\phi-\theta)}{g\cos^2\phi\cos\theta}. \tag{D4}$$

Upon expanding $\sin(\phi-\theta)$ and $\cos(\phi-\theta)$ using difference formulae, algebra and trigonometric identities eventually lead to

10   $$\lambda = \frac{2v_0^2\cos\theta}{g}\tan\phi(1 + \tan\phi\tan\theta$$

$$+\tan^2\theta + \tan\phi\tan^3\theta) \tag{D5}$$

For $\theta = 0$, this reduces to $\lambda = 2v_0^2\tan\phi/g$. If for small slopes $\tan\phi \sim \tan\theta$ and for large slopes $\tan\phi \ll \tan\theta$, then at leading order,

15   $$\lambda \approx \frac{2v_0^2\cos\theta}{g}\tan\phi(1 + \tan^2\theta) = \frac{2v_0^2\tan\phi}{g\cos\theta} \tag{D6}$$

For the purpose of scaling, we now assume that $v_0^2 \sim \langle u^2 \rangle$ and write

$$\lambda \approx \frac{2\langle u^2 \rangle \tan\phi}{g\cos\theta} \tag{D7}$$

which gives Eq. (26) in the text. The soft matter trajectory analysis of Tajima and Fujisawa (2020) includes viscous air resistance, which we neglect.

Appendix E: Energy extraction during collisions

Here we provide a qualitative description of the basis for assuming that a change in the downslope energy of a particle associated with a collision can be expressed as $\Delta E_p = -\beta_x E_p$ wherein both β_x and ΔE_p must be treated as random variables. We start by noting that the topic of particle collision mechanics is well developed for idealized particle-particle collisions and

5 particle-surface collisions involving spherical particles, as well as peculiarities of non-collinear collisions associated with irregular particles. Relevant elements are covered in Brach (1984, 1989, 1991), Stronge (1990, 2000), Brach and Dunn (1992, 1995) and Ismail and Stronge (2008). Although we cannot directly apply details of this work given the complexity of particle motions on natural rough hillslopes, this work nonetheless offers a clear guide in the interpretation of the relation $\Delta E_p = -\beta_x E_p$, notably in relation to experimental results presented in the second companion paper (Furbish et al., 2020a).

With reference to Figure E1, consider an idealized collision of a spherical particle with a rigid planar surface with slope
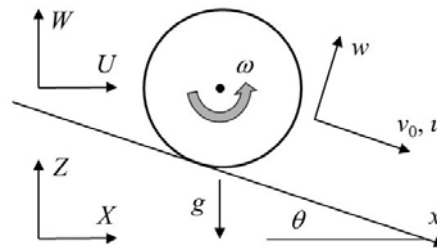

Figure E1. Definition diagram for idealized collision of a spherical particle with a rigid planar surface.

10

angle θ. Let u, w and ω respectively denote the surface parallel velocity, the surface normal velocity and the angular velocity of the particle with mass m and radius $r = D/2$, and let the subscripts 1 and 2 denote incident and reflection values. With appropriate modification of the coordinate and sign convention used by Brach (1991), the momentum components associated with impulses can be expressed as (Brach, 1991; Brach and Dunn, 1995; Brach, 1998)

15
$$w_2 = -\epsilon w_1 , \tag{E1}$$

$$u_2 = u_1 + \mu_c(1+\epsilon)w_1 + g\tau(\sin\theta - \mu_c\cos\theta) \quad \text{and} \tag{E2}$$

$$\omega_2 = \omega_1 + \frac{5}{2}\frac{\mu_c}{r}[(1+\epsilon)w_1 - g\tau\cos\theta] , \tag{E3}$$

20 where $w_1 < 0$, ϵ is the normal coefficient of restitution attributed to Newton, μ_c is the ratio of tangential to normal impulses during the collision, and τ is the impulse duration. Note that μ_c generally is not a coefficient of friction, although it may be equal to a coefficient of friction in special cases, for example, with sliding throughout the entire duration of the collision (Brach, 1991; Brach and Dunn, 1992). Also note that $\mu_c = 0$ if $u_1 = 0$.

The second term on the right side of Eq. (E2) represents the effect of tangential friction on the velocity u, increasing with the magnitude of the normal impulse associated with the velocity w_1. This term may be considered the dynamic contribution to friction during τ. The term $g\tau\sin\theta$ represents the downslope contribution to the impulse associated with the weight of the particle, and the term $g\tau\mu_c\cos\theta$ represents an enhancement of friction associated with this weight. The impulse duration τ

5 may be on the order of milliseconds for a hard particle impacting a hard surface. It may be longer for a hard particle impacting a relatively soft surface (Brach, 1991). If the magnitude of w_1 is sufficiently large and τ is sufficiently short, the gravitational terms in Eq. (E2) and Eq. (E3) may be neglected. The second term on the right side of Eq. (E3) represents the effect of tangential friction in contributing to rotational motion, that is, the conversion of translational energy to rotational energy.

Collisions involving small incident angles begin with sliding during the impulse duration τ. If with a sufficient normal

10 dynamic force this initial sliding gives way to stick prior to separation, then for a sphere with moment of inertia $I = (2/5)mr^2$, the velocity $u_2 = r\omega_2$ at separation. This leads to

$$u_2 = \frac{u_1 + g\tau\sin\theta}{1+2/5}, \tag{E4}$$

which represents the outcome of a conversion of translational to rotational motion with stick. Whereas the resultant velocity u_2 can be determined in this situation, the effect of sliding on u_2 cannot be analytically constrained. Nonetheless, Eq. (E3)

15 indicates that collisions induce a conversion of translational to rotational motion in that tangential friction during an impulse exerts a torque on the particle, thereby extracting translational kinetic energy that is in addition to work performed during particle deformation and by friction. We also note that low-angle collisions likely dominate in the problem at hand.

In order to recast the problem in terms of kinetic energy, we start by squaring Eq. (E1), Eq. (E2) and Eq. (E3) to give

$$w_2^2 = \epsilon^2 w_1^2, \tag{E5}$$

20

$$u_2^2 = u_1^2 + 2\mu_c(1+\epsilon)u_1 w_1 + u_c^2(1+\epsilon)^2 w_1^2$$

$$+2g\tau(\sin\theta - \mu_c\cos\theta)u_1$$

25 $$+2\mu_c(1+\epsilon)g\tau(\sin\theta - \mu_c\cos\theta)w_1$$

$$+g^2\tau^2(\sin\theta - \mu_c\cos\theta) \quad \text{and} \tag{E6}$$

$$\omega_2^2 = \omega_1^2 + 5\frac{\mu_c}{r}(1+\epsilon)\omega_1 w_1 + \frac{25}{4}\frac{\mu_c^2}{r^2}(1+\epsilon)^2 w_1^2$$

30 $$-5\frac{\mu_c}{r}g\tau\cos\theta\omega_1 - \frac{25}{2}\frac{\mu_c^2}{r^2}g\tau\cos\theta w_1$$

$$+\frac{25}{4}\frac{\mu_c^2}{r^2}g^2\tau^2\cos^2\theta. \tag{E7}$$

In addition we square Eq. (E4) to give

$$u_2^2 = \frac{25}{49}u_1^2 + \frac{50}{49}g\tau\sin\theta u_1 + \frac{25}{49}g^2\tau^2\sin^2\theta. \tag{E8}$$

We may immediately neglect terms involving τ^2, and for sufficiently large w_1 and small τ we may neglect terms involving τ.

The next task involves scaling the normal velocity w_1 in terms of the tangential velocity u_1 in relation to particle motions down an inclined surface. Hereafter we focus on lowest order effects. With reference to the analysis presented in Appendix D, let W_0 denote the vertical reflection velocity of a particle following a collision. Assuming downslope motion, then for any finite horizontal reflection velocity U_0 and reflection angle ϕ, the magnitude of the vertical velocity at the next collision is given by

$$\frac{1}{2}mW_1^2 = \frac{1}{2}mW_0^2 - mgZ, \tag{E9}$$

where $Z \leq 0$ is the vertical distance between the collisions. That is,

$$W_1 = -\sqrt{W_0^2 - 2gZ}. \tag{E10}$$

From Appendix D, $W_0 = v_0\sin(\phi-\theta)/\cos\phi$, $Z = -\frac{1}{2}gt_0^2 + W_0t_0$ and $t_0 = 2W_0/g + 2SW_0/g$, where v_0 is the surface parallel velocity associated with W_0, t_0 is the travel time and $S = \tan\theta$. Using these relations with Eq. (E10) we obtain

$$W_1 = -\frac{v_0}{\cos\phi}\Big[\sin^2(\phi-\theta) + 4S^2\cos^2(\phi-\theta)$$

$$+ 4S\cos(\phi-\theta)\sin(\phi-\theta)\Big]^{1/2}. \tag{E11}$$

Expanding the trigonometric functions in Eq. (E11) as Taylor series and retaining the lowest order term in ϕ we obtain

$$w_1 = W_1\cos\theta \approx -\frac{\cos\theta\sin\theta}{\cos\phi}v_0. \tag{E12}$$

In effect the magnitude of w_1 is set by the gain in the magnitude of the vertical velocity associated with conversion of gravitational potential energy to translational energy with finite slope. This strengthens the normal impulse of the particle, but only up to a slope (nominally 45 degrees) beyond which the surface normal component of the vertical velocity begins to decrease.

As in Appendix D we now scale $u_1 \sim v_0$. Using Eq. (E12), at lowest order Eq. (E6) becomes

$$u_2^2 \approx u_1^2 - \frac{2\mu_c(1+\epsilon)\cos\theta\sin\theta}{\cos\phi}u_1^2. \tag{E13}$$

Subtracting u_1^2 from both sides of Eq. (E13) and multiplying by $m/2$,

$$\frac{1}{2}m(u_2^2 - u_1^2) \approx -\frac{2\mu_c(1+\epsilon)\cos\theta\sin\theta}{\cos\phi}\frac{1}{2}mu_1^2. \tag{E14}$$

Omitting subscripts, this is

$$\Delta E_p \approx -\frac{2\mu_c(1+\epsilon)\cos\theta\sin\theta}{\cos\phi}E_p. \tag{E15}$$

Comparing this result with the assumption $\Delta E_p = -\beta_x E_p$, we may conclude that

$$\beta_x \sim \frac{2\mu_c(1+\epsilon)\cos\theta\sin\theta}{\cos\phi}\,. \tag{E16}$$

Note that Eq. (E15) and Eq. (E16) pertain to a highly idealized collision. In fact, the quantities μ_c, ϵ and ϕ are each random variables. Moreover, on an irregular hillslope surface the angle θ also is a random variable when viewed at the particle-surface collision scale. Nonetheless, for the purpose of scaling we may view this angle as a locally averaged value, and we now take the ensemble average of Eq. (E16) to give

$$\langle\beta_x\rangle \sim \left\langle\frac{2\mu_c(1+\epsilon)}{\cos\phi}\right\rangle\cos\theta\sin\theta\,. \tag{E17}$$

In turn, with $\mu = \langle\beta_x\rangle/4\tan\phi$ we may write

$$\mu \sim M(\theta)\,, \tag{E18}$$

with

$$M(\theta) = \left\langle\frac{2\mu_c(1+\epsilon)}{4\sin\phi}\right\rangle\cos\theta\sin\theta\,. \tag{E19}$$

At lowest order, $\cos\theta\sin\theta \sim \theta$. We therefore may expect μ to systematically vary with the slope angle θ. Also note that μ is independent of particle size. We examine both of these points in the second companion paper (Furbish et al., 2020a).

Subtracting u_1^2 from both sides of Eq. (8), multiplying by $m/2$ and retaining the lowest order term,

$$\frac{1}{2}m(u_2^2 - u_1^2) \approx -\left(1 - \frac{25}{49}\right)\frac{1}{2}mu_1^2\,. \tag{E20}$$

This is

$$\Delta E_p \approx -0.5 E_p\,. \tag{E21}$$

This result indicates that the onset of rotation with stick produces a large change in the slope-parallel kinetic energy. In this case, $\beta_x \approx 0.5$. Again notice that this result is independent of particle size. Nonetheless, the numerical factors in Eq. (4), Eq. (8) and Eq. (E20) are set by the moment of inertia of the particle, which means that these factors vary with irregular particles. Also note that Eq. (E21) does not imply that half of the translational energy E_p is converted entirely to rotational energy. Rather, half is converted to rotational energy *and* lost to work performed by friction prior to stick and by particle/surface deformation, thence dissipated as heat, vibrations and sound.

More generally, with low incident angle motions, slip is more likely. Focusing on the first three terms on the right side of Eq. (E7) and using Eq. (E12) with $v_0 \sim u_1$,

$$\omega_2^2 = \omega_1^2 - 5\frac{\mu_c}{r}(1+\epsilon)\frac{\cos\theta\sin\theta}{\cos\phi}\omega_1 w_1$$

$$+\frac{25}{4}\frac{\mu_c^2}{r^2}(1+\epsilon)\frac{\cos^2\theta\sin^2\theta}{\cos^2\phi}u_1^2\,. \tag{E22}$$

Subtracting ω_1^2 from both sides of Eq. (E22) and multiplying by $I/2 = (1/5)mr^2$,

$$\frac{1}{2}I(\omega_2^2 - \omega_1^2) = -m\mu_c r(1+\epsilon)\frac{\cos\theta\sin\theta}{\cos\phi}\omega_1 u_1$$

$$+\frac{5}{2}\mu_c^2(1+\epsilon)\frac{\cos^2\theta\sin^2\theta}{\cos^2\phi}\frac{1}{2}mu_1^2, \tag{E23}$$

5   which is

$$\Delta E_r = \frac{5}{2}\mu_c^2(1+\epsilon)\frac{\cos^2\theta\sin^2\theta}{\cos^2\phi}E_p$$

$$+\sqrt{10}\mu_c(1+\epsilon)\frac{\cos\theta\sin\theta}{\cos\phi}\sqrt{E_r}\sqrt{E_p}. \tag{E24}$$

This result suggests that in the absence of initial rotation ($E_r = 0$), a change in rotational energy is directly related to the

10   translational energy E_p, where the proportion β_x now represents the leading factors in the first term on the right side of Eq. (E24). With extant rotational motion, a weaker conversion of translational to rotational energy occurs according to the second term on the right side. Both cases are slope dependent due to the connection between w_1 and $u_1 \sim v_0$ implied by Eq. (E12).

Focusing on downslope motions, in general we may write the energy balance of a particle as

$$\Delta E_p = -\Delta E_r - f_c - f_y. \tag{E25}$$

15   Here, a positive change in rotational energy ΔE_r is seen as an extraction of translational energy. Then, for example, this loss is given explicitly by Eq. (E20) in the specific case of stick with the onset of rotation. An approximation of this loss is given by Eq. (24) for a frictional collision that does not necessarily involve stick. The term f_c in Eq. (E25) represents losses associated with particle and surface deformation as well as work performed against friction during collision impulses (converted to heat, sound, etc.). This is represented, for example, by Eq. (15). But this term also includes losses associated with deformation of the surface

20   at a scale larger than that of an idealized particle-surface impulse contact, namely, due to momentum exchanges associated with the sputtering of loose surface particles during collision. (The videos published as supplementary material to DiBiase et al. (2017) nicely illustrate this sputtering as well as the onset of rotational motion.) The term f_y in Eq. (E25) represents energy losses not described in the preceding idealized formulation, namely, changes in downslope translational energy associated with glancing collisions that produce transverse translational motions and rotational motions oriented differently than that

25   considered above (Figure E1). In some cases, as described above, the change in energy ΔE_p can be expressed directly in terms of the energy state E_p. However, the complexity of particle-surface collisions on natural hillslopes precludes explicitly demonstrating such a relation for all possible scenarios. Nonetheless, the examples above suggest that it is entirely defensible to assume that energy losses can be related to the energy state E_p if the elements involved are formally viewed as random variables. Specifically, with the effect of slope angle θ on the impact velocity w_1 and its relation to $u_1 \sim v_0$ via Eq. (E12), we

30   can be confident that the loss ΔE_p is functionally related to the energy state E_p. The simple relation $\Delta E_p = -\beta_x E_p$ thus is to be viewed as an hypothesis to be tested against data, as elaborated in the second companion paper (Furbish et al., 2020a).

Appendix F: Product of averages

Let E_{p_i} denote a discrete value of the particle energy. Our objective is to show that the product $\langle E_{pi}\rangle\langle 1/E_{pi}\rangle \geq 1$. We start by writing this inequality as

$$\left(\frac{1}{N}\sum_{i=1}^{N} E_{pi}\right)\left(\frac{1}{N}\sum_{i=1}^{N}\frac{1}{E_{pi}}\right) \geq 1. \tag{F1}$$

5   This means that

$$\frac{1}{N}\sum_{i=1}^{N} E_{pi} \geq \frac{N}{\sum_{i=1}^{N}\frac{1}{E_{pi}}}. \tag{F2}$$

Whereas the left side of Eq. (F2) is the arithmetic average E_a, the right side is the harmonic average E_h. Thus,

$$\frac{E_a}{E_h} \geq 1. \tag{F3}$$

Because the arithmetic average of a set of positive numbers is always greater than or equal to the harmonic average of this set,
10   this inequality is indeed satisfied. These averages are equal only if all values of the set are equal, that is, the variance of the set is zero.

We do not know the form of the underlying distribution $f_{E_p}(E_p, x)$. For physical reasons, however, it cannot be a distribution that supports $E_p \to 0$, as this coincides with particles at rest. For example, $f_{E_p}(E_p, x)$ cannot be an exponential or Weibull distribution with support $E_p \in [0, \infty)$. In contrast, the lognormal and gamma distributions with support $E_p \in (0, \infty)$
15   are admissible, and the Pareto distribution with support $E_p \in [E_{pm}, \infty)$ is admissible.

As a point of reference, for a density $f_{E_p}(E_p)$ with finite expected value $\langle E_p\rangle$, the density $f_y(y)$ of the reciprocal $y = 1/E_p$ may not have defined moments. This occurs, for example, if $f_{E_p}(E_p)$ is exponential with support $E_p \in [0, \infty)$. Interestingly, if with $x = \ln(E_p)$ the density $f_x(x)$ is lognormal with mean μ, then with $y = 1/x$ the density $f_y(y)$ also is lognormal with mean $-\mu$.

20   For a density $f_y(y)$ of $y = 1/E_p$ with undefined mean, the average $\langle y\rangle$ calculated from a sample nonetheless is finite, as the probability of sampling precisely a value $E_p = 0$ is identically zero. Moreover, as the variance of E_p becomes small for finite mean $\langle E_p\rangle$, the product $\langle E_p\rangle\langle y\rangle = \langle E_p\rangle\langle 1/E_p\rangle \to 1$, as in the discrete case above.

Appendix G: Deposition rate

Our description of the deposition rate for a granular gas in a box has both similarities and dissimilarities with the processes of
25   deposition (de-sublimation) and condensation. Here we briefly outline key points.

In a closed system involving two phases (solid/gas or solid/liquid) at thermodynamic equilibrium, the rates of deposition and sublimation (or condensation and evaporation) are equal. That is, the rate at which molecules move from the solid phase to the gas phase (or from the liquid phase to the gas phase) is balanced by the rate at which molecules move from the gas phase to the solid phase (or from the gas phase to the liquid phase). These rates, in each direction, depend only on the thermal state

of the system. Because the system has specified internal energy involving conservative particle-particle collisions, we do not need to appeal to the idea of heating and cooling (although this could be occurring). For a granular gas involving dissipative collisions, however, a non-equilibrium steady state is achieved only if it is continuously mechanically heated, and the rate of heating is matched by the rate of cooling due to the collisions. (Note that we refer to a non-equilibrium steady state condition

5   rather than thermal equilibrium, as unlike an ordinary gas, a granular gas can exhibit strong spatial correlations in the particle number density (see Brilliantov and Pöschel (2004, 2005) and Brilliantov et al. (2018) and references therein; and van Zon and MacKintosh, (2004)). However, this distinction is unimportant in relation to the behavior of particle motions on a hillslope envisioned as a rarefied granular gas.) Like an ordinary solid-gas system, the rate of sublimation (entrainment) is matched by the rate of deposition (disentrainment), and the total particle energy and the average particle energy are fixed. Moreover, like

10   an ordinary solid-gas system, the deposition rate depends on the physics of disentrainment in relation to its thermal state, not on the difference between the heating and cooling rates (which is zero at steady state). Heating modulates the deposition rate as described in the text.

Appendix H: Generalized Pareto distribution

Solving Eq. (65) gives

15   $$\hat{E}_a(\hat{x}) = \left[Ki - 1 + \frac{1}{\alpha}(\gamma - 1) \right] \hat{x} + \hat{E}_{a0} \,. \tag{H1}$$

Using Eq. (64) the disentrainment rate is then

$$\hat{P}_{\hat{x}}(\hat{x}) = \frac{1}{(\alpha/\gamma)(Ki + \gamma/\alpha - 1/\alpha - 1)\hat{x} + \alpha\hat{E}_{a0}/\gamma} \,, \tag{H2}$$

which we write as

$$\hat{P}_{\hat{x}}(\hat{x}) = \frac{1}{a\hat{x} + b} \,. \tag{H3}$$

20   Making use of Eq. (4) we then obtain the distribution of travel distances, namely,

$$f_{\hat{x}}(\hat{x}) = \frac{b^{1/a}}{(a\hat{x} + b)^{1+1/a}} \,. \tag{H4}$$

This is a generalized Pareto distribution with location parameter equal to zero.

To show how the generalized Pareto distribution is related to the ordinary Lomax distribution, we start by rewriting Eq. (H4) as

25   $$f_{\hat{x}}(\hat{x}) = \frac{b^{1/a}}{a^{1+1/a}(\hat{x} + b/a)^{1+1/a}} \,. \tag{H5}$$

This is

$$f_{\hat{x}}(\hat{x}) = \frac{(1/a)(b/a)^{1/a}}{(\hat{x} + b/a)^{1+1/a}} \,. \tag{H6}$$

We now define the shape parameter $a_L = 1/a$ and the scale parameter $b_L = b/a$. This gives a Lomax ditribution, namely,

$$f_{\hat{x}}(\hat{x}) = \frac{a_L b_L^{a_L}}{(\hat{x} + b_L)^{1+a_L}}. \tag{H7}$$

Thus, for $a > 0$ the behavior of the generalized distribution, Eq. (H4), is the same as that of a Lomax distribution. The mean is

$$\mu_{\hat{x}} = \frac{b_L}{a_L - 1} \qquad a_L > 1. \tag{H8}$$

5   We work with the generalized Pareto distribution in the form of Eq. (H4) because of the clear connection between its parameters and the disentrainment rate function, Eq. (H3), and because the condition $a < 0$ is physically meaningful.

Appendix I: Kirkby-Statham formulation

The formulation of Kirkby and Statham (1975) assumes that initial particle kinetic energy is dissipated in work performed by a fixed Coulomb-like friction to give an average travel distance. This idea can be formulated in terms of momentum and energy,

10   then recast in terms of the rate of change in energy with respect to position x for comparison with the formulation presented in the main text.

In appealing to a Coulomb-like friction behavior, Kirkby and Statham (1975) start with $F_x = mg\sin\theta - \mu_d mg\cos\theta$. With particle velocity u we write this as

$$\frac{\mathrm{d}u(t)}{\mathrm{d}t} = g\sin\theta - \mu_d g\cos\theta. \tag{I1}$$

15   Note that $u(t)$ must be envisioned as representing an idealized "average" velocity of a group of particles viewed over time. This gives

$$u(t) = (g\sin\theta - \mu_d g\cos\theta)t + u_0. \tag{I2}$$

For a total travel time T,

$$u_p(T) = 0 = (g\sin\theta - \mu_d g\cos\theta)T + u_0, \tag{I3}$$

20   so that

$$T = -\frac{u_0}{g\sin\theta - \mu_d g\cos\theta}. \tag{I4}$$

In turn we rewrite Eq. (I2) as

$$\frac{\mathrm{d}x(t)}{\mathrm{d}t} = (g\sin\theta - \mu_d g\cos\theta)t + u_0, \tag{I5}$$

so that

25    $$x(t) = \frac{1}{2}(g\sin\theta - \mu_d g\cos\theta)t^2 + u_0 t. \tag{I6}$$

The total travel distance X is thus

$$x(T) = X = -\frac{u_0^2}{g\sin\theta - \mu_d g\cos\theta}\,. \tag{I7}$$

Using the initial squared velocity $u_0^2 = \epsilon^2 gh\sin^2\theta$,

$$X = -\frac{\epsilon^2 h\sin^2\theta}{\sin\theta - \mu_d\cos\theta}\,. \tag{I8}$$

5 This is the result that Kirkby and Statham (1975) offer as representing the average travel distance.

We now turn to kinetic energy. Let $A = g\sin\theta - \mu_d g\cos\theta$. Multiplying Eq. (I1) by mu then leads to

$$\frac{\mathrm{d}}{\mathrm{d}t}\left(\frac{m}{2}u^2\right) = \frac{\mathrm{d}E_p}{\mathrm{d}t} = mAu\,. \tag{I9}$$

With $u = At + u_0$ from Eq. (I3),

$$\frac{\mathrm{d}E_p}{\mathrm{d}t} = mA^2 t + mAu_0\,. \tag{I10}$$

10 This leads to

$$E_p(t) = \frac{1}{2}mA^2 t^2 + mAu_0 t + E_{p0}\,. \tag{I11}$$

We now solve Eq. (I6) for t in terms of x to give

$$t = \frac{1}{2A}\left(-2u_0 + \sqrt{4u_0^2 + 8Ax}\right)\,. \tag{I12}$$

Substituting this into Eq. (I11) and doing algebra then yields $E_p(x) = mAx + E_0$. The derivative of this result with respect to

15 x is

$$\frac{\mathrm{d}E_p(x)}{\mathrm{d}x} = mg\sin\theta - \mu_d mg\cos\theta\,. \tag{I13}$$

This result is like Eq. (57), but absent the effect of deposition and the associated apparent heating, as it strictly applies to the motion of an individual particle or a group of particles acting like a rigid body. It does not describe an ensemble averaged motion.

20 **Appendix J: Gabet-Mendoza formulation**

Gabet and Mendoza (2012) appeal to ideas from Samson et al. (1998) and Quartier et al. (2000) and suggest that the motion of an individual particle can be described as

$$\frac{\mathrm{d}u(t)}{\mathrm{d}t} = g\sin\theta - \mu_d g\cos\theta - \kappa u^\psi\,. \tag{J1}$$

However, whereas the derivative term on the left side of Eq. (J1) and the first two terms on the right side pertain to the

25 instantaneous motion of an individual sliding particle or group of particles acting like a rigid body, the third term on the

right side, representing collisional friction, actually is relevant to time-averaged or ensemble-averaged behavior rather than the instantaneous behavior of an individual particle (Riguidel et al., 1994a, 1994b; Samson et al., 1998, 1999). These terms are not additive as written. The gravity and Coulomb friction terms are like those in the formulation of Kirkby and Statham (1975). Because there is confusion in the literature regarding the collisional friction term, here we elaborate its form.

5   Let n_t denote the expected number of particle-surface interactions (collisions) per unit time as a particle moves downslope, and let β_x denote the proportion of momentum parallel to x that is extracted during an individual collision involving the particle velocity u. Recognizing that both β_x and u must be treated as random variables, and letting angle brackets denote an ensemble average, we may now assume that

$$m\frac{\mathrm{d}\langle u \rangle}{\mathrm{d}t} \approx mg\sin\theta - mn_t\langle \beta_x u \rangle. \tag{J2}$$

10 The first term on the right side of Eq. (J2) represents the uniform gravitational force, and the second term on the right side represents a frictional force due to particle-surface collisions (compare with Eq. (2) in Riguidel et al., 1994). As a reminder, this term is entirely analogous to the dissipation term that Haff (1983) introduced (formulated in terms of energy rather than momentum), leading to Haff's cooling law (Brilliantov and Pöschel, 2004; Yu et al., 2020). The proportion of momentum extracted, β_x, involves an appropriate coefficient of restitution depending on the geometrical details of the collision. We may

15 now assume that $n_t \sim \langle u \rangle/l$, where l denotes a characteristic length scale representing the expected distance between collisions. This leads to

$$\frac{\mathrm{d}\langle u \rangle}{\mathrm{d}t} \approx g\sin\theta - \frac{1}{l}\langle \beta_x u \rangle\langle u \rangle, \tag{J3}$$

which is close to the form of Eq. (J1) with $\psi = 2$ (neglecting the Coulomb friction term), but not quite.

We now focus on uniform, steady conditions such that $\langle u \rangle$ is unchanging with position or time, consistent with various

20 experiments (Riguidel et al., 1994; Samson et al., 1998). This leads to

$$\langle \beta_x u \rangle\langle u \rangle \approx lg\sin\theta. \tag{J4}$$

We now write $\beta_x = \langle \beta_x \rangle + \beta_x'$ and $u = \langle u \rangle + u'$, where primes denote deviations about the expected values. Substituting these expressions into Eq. (J4) and taking expected values then leads to

$$\langle \beta_x \rangle\langle u \rangle^2 + \langle \beta_x' u' \rangle\langle u \rangle \approx lg\sin\theta. \tag{J5}$$

25 The product $\langle \beta_x \rangle\langle u \rangle^2$ has the appearance of a nominal, nonlinear viscous term. Samson et al. (1998) suggest that this represents a Bagnold-like friction based on analogy with the scaling provided by Bagnold (1954), preceding the critical assessment of Bagnold's experimental work presented by Hunt et al. (2002). The term $\langle \beta_x' u' \rangle\langle u \rangle$, neglected at the outset by Riguidel et al. (1994), looks like a linear viscous term, where the "viscosity" is given by the covariance $\langle \beta_x' u' \rangle$.

Noting that Eq. (J5) is quadratic, we can solve for the velocity $\langle u \rangle$ and determine that at lowest order

30 $$\langle u \rangle \approx \left(\frac{lg\sin\theta}{\langle \beta_x \rangle}\right)^{1/2}, \tag{J6}$$

so long as $(\langle\beta'_x u'\rangle/\langle\beta_x\rangle)^2 < 4lg\sin\theta/\langle\beta_x\rangle$. If this inequality is satisfied, then Eq. (J3) becomes

$$\frac{d\langle u\rangle}{dt} \approx g\sin\theta - \frac{1}{l}\langle\beta_x\rangle\langle u\rangle^2,\tag{J7}$$

giving $\psi = 2$. Note that the squared average velocity in Eq. (J7) does not imply that collisional friction is scaled with kinetic energy rather than momentum. This result occurs because n_t is initially scaled with $\langle u\rangle$ and l. Quartier et al. (2000) present

5 an analogous formulation; see their Eq. (4) and explanation of the squared velocity term. Dippel et al. (1997) also discuss this point.

In relation to their experiments involving particles of radius R moving down an inclined surface roughened with a quasi-random monolayer of particles with radius r_m, Riguidel et al. (1994) and Samson et al. (1998) propose the hypothesis that $\langle u\rangle \sim \sin\theta$. This derives from a scaling analysis in which the magnitude of the collisional momentum extraction (i.e., $\langle\beta_x\rangle$) is

10 written as a function of the relative smoothness R/r_m by introducing an unconstrained velocity quantity. These authors plot measured values of $\langle u\rangle$ versus $\sin\theta$ and suggest that the linear fit confirms a viscous-like behavior. Note, however, that because of the rather limited experimental range of $\sin\theta$ (Figure 2 in Riguide et al., 1994; Figure 2 in Samson et al., 1998; Figure 4 in Samson et al., 1999), the data are equally well fit by a straight line in a plot involving $\sqrt{\sin\theta}$ (Figure J1), consistent with the
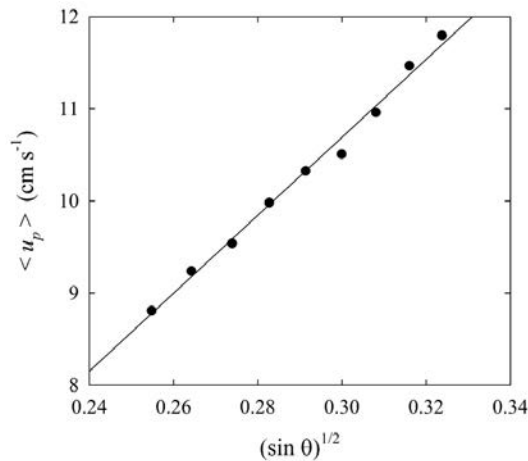

Figure J1. Plot of ensemble averaged particle velocity $\langle u\rangle$ versus $\sqrt{\sin\theta}$ involving a steel sphere ($R = 2.5$ mm) moving over glass beads ($r_m = 0.53$ mm) giving $R/r_m = 4.7$; data from Samson et al. (1998).

collisional-based formulation, Eq. (J7). (Sampson et al. (1999) acknowledge this limitation of the range of $\sin\theta$.) In addition,

15 we can scale the length l as $l \sim r_m/c_A$, where $c_A = 0.67$ is the areal concentration of the surface-roughness particles. For a fixed velocity $\langle u\rangle$, Eq. (J7) gives $l \approx \langle\beta_x\rangle\langle u\rangle^2/g\sin\theta$. With $R/r_m = 4.7$ and a coefficient of restitution of $\epsilon \approx 0.8$, we can estimate $\langle\beta_x\rangle \approx 0.05$. This gives $l \approx 0.5 - 0.6$ mm over the range of measured velocities in Figure J1, which is close to the experimental value of $l = r_m/c_A = 0.8$ mm, thereby reinforcing the collisional basis of Eq. (J7). Thus, a spherical particle that macroscopically rolls over a monolayer roughness is actually going bumpety-bump, colliding with monolayer particles during

20 its motion.

Because the relative smoothness R/r_m is not entirely adequate in scaling the collisional friction as c_A varies (Samson et al., 1998), it remains unclear whether these experimental conditions involve an apparent viscous-like behavior where the effective viscosity depends only on roughness geometry (Dippel et al., 1997; Samson et al., 1999) or a squared-velocity behavior as in Eq. (J7). Dippel et al. (1997) note that there is an apparent cross-over in behavior for very large and heavy spheres. Effects of
5   the covariance of β_x and u in relation to roughness geometry and the details of motions, including transverse motions, likely are important. Nonetheless, we emphasize that in the formulations of Riguidel et al. (1994) and Samson et al. (1998), a Coulomb friction behavior is not involved.

Returning to Eq. (J1), similarly there is no clear reason to include a Coulomb-like friction term, as natural irregular particles mostly do not slide down natural rough surfaces. In addition, if the starting point involves the derivative term on the left side
10   and the gravitational term on the right side as written, then the collisional term on the right side should be a random quantity, thus leading to a stochastic differential equation — that is, a Langevin-like equation (Riguidel et al., 1994) — not an ordinary differential equation. Moreover, the idea of a dynamic friction coefficient is misapplied in the situation where rarefied particles tumble, roll and skitter over the surface. A Coulomb model is appropriate for sustained contact, and even then a dynamic friction involves collisional friction at the surface asperity scale. Particle-surface contacts on natural granular surfaces are not
15   smooth at a scale commensurate with a sliding Coulomb model. A rolling coefficient of friction works for spheres moving over a relatively smooth surface, not for irregular tumbling particles involving non-collinear impacts. Moreover, the static normal weight of a particle, $mg\cos\theta$, does not set the particle-surface friction. Rather, dynamic forces during collision impulses matter (Brach, 1991; Stronge, 2000). This includes the dynamic Coulomb friction force associated with conversion of translational to rotational kinetic energy during collisions (Appendix E). Any resulting dynamic friction coefficient represents an ensemble
20   averaged ratio of tangential to normal momentum exchanges, both of which are random variables. (This point currently is being examined in studies of bed load and aeolian transport; see for example Pähtz and Duran (2018).) Finally, the experiments of Quartier et al. (2000) involved rolling a cylinder over an inclined row of cylinders in an experiment designed to remove the transverse degree of freedom of motion. The Coulomb-like term in their formulation (see their Eq. (5)) arises from trapping of the rolling cylinder between bumps, and is unrelated to sliding as in a conventional Coulomb model.

25   *Author contributions.* All authors contributed to the conceptualization of the problem and its technical elements. DJF wrote much of the paper with contributions by the other authors. Because AMA is deceased, we offer the following clarification. AMA made key observations regarding particle motions in initial laboratory experiments during her MS work, and worked closely with DJF in conceptualizing a description of these motions. Whereas we did not succeed in formalizing AMA's ideas in mathematical terms while she was pursuing her work, these ideas were essential to a proper description of particle motions and are now formalized in the paper. We also note that AMA's co-authorship
30   carries full approval of her family.

Competing interests. We have no competing interests.

References

Ancey, C., Davison, A., Böhm, T., Jodeau, M., and Frey, P.: Entrainment and motion of coarse particles in a shallow water stream down a steep slope, Journal of Fluid Mechanics, 595, 83–114, 2008.

Anderson, R. S.: Modeling the tor-dotted crests, bedrock edges, and parabolic profiles of high alpine surfaces of the Wind River Range, Wyoming, Geomorphology, 46, 35–58, 2002.

Atwood-Stone, C. and McEwen, A. S.: Avalanche slope angles in low-gravity environments from active Martian sand dunes, Geophysical Research Letters, 40, 2929–2934, 2013.

Bagnold, R. A.: Experiments on a gravity-free dispersion of large solid spheres in a Newtonian fluid under shear, Proceeding of the Royal Society of London A, 225, 49–63, 1954.

Baldassarri, A., Barrat, A., D'Anna, G., Loreto, V., Mayor, P., and Puglisi, A.: What is the temperature of a granular medium, Journal of Physics: Condensed Matter, 17, S2405–S2428, doi: 10.1088/0953-8984/17/24/003, 2005.

Bendror, E. and Goren, L.: Controls over sediment flux along soil-mantled hillslopes: Insights from granular dynamics simulations, Journal of Geophysical Research – Earth Surface, 123, 924–944, https://doi.org/10.1002/2017jf004351, 2018.

Bocquet, L., Colin, A., and Ajdari, A.: Kinetic theory of plastic flow in soft glassy materials, Physical Review Letters, 103, 036001, 2009.

Brach, R. M.: Friction, restitution, and energy loss in planar collisions, Journal of Applied Mechanics, 51, 164–170, 1984.

Brach, R. M.: Rigid body collisions, Journal of Applied Mechanics, 56, 133–138, 1989.

Brach, R. M.: Mechanical Impact Dynamics, John Wiley, New York, 1991.

Brach, R. M.: Formulation of rigid body impact problems using generalized coefficients, International Journal of Engineering Science, 36, 61–71, 1998.

Brach, R. M. and Dunn, P. F.: A mathematical model of the impact and adhesion of microsphers, Aerosol Science and Technology, 16, 51–64, 1992.

Brach, R. M. and Dunn, P. F.: Macrodynamics of microparticles, Aerosol Science and Technology, 23, 51–71, 1995.

Brantov, A. V. and Bychenkov, V. Yu.: Nonlocal transport in hot plasma. Part I, Plasma Physics Reports, 39, 698–744, 2013.

Brilliantov, N. V. and Pöschel, T.: Kinetic Theory of Granular Gases, Oxford University Press, New York, 2004.

Brilliantov, N. V. and Pöschel, T.: Self-diffusion in granular gases: Green-Kubo versus Chapman-Enskog, Chaos, 15, 026108, 2005.

Brilliantov, N. V., Formella, A., and Pöschel, T.: Increasing temperature of cooling granular gases, Nature Communications, 9, 797, doi: 10.1038/s41467-017-02803-7, 2018.

Cates, M. E., Wittmer, J. P., Bouchaud J-P., and Claudin, P.: Jamming, force chains, and fragile matter, Physical Review Letters, 81, 1841–1844, 1998.

Chandrasekhar S.: Stochastic problems in physics and astronomy, Reviews of Modern Physics, 15, 1–89, 1943.

Culling, W. E. H.: Soil creep and the development of hillside slopes, Journal of Geology, 71, 127–161, 1963.

Daniels, K. E. and Behringer, R. P: Characterization of a freezing/melting transition in a vibrated and sheared granular medium, Journal of Statistical Mechanics, P07018, doi: 10.1088/1742-5468/2006/07/P07018, 2006.

Deshpande, N. S., Furbish, D. J., Arratia, P. E., and Jerolmack, D. J.: The perpetual fragility of creeping hillslopes, https://doi.org/10.31223/osf.io/qc9jh, 2020. (in review)

DiBiase, R. A. and Lamb, M. P.: Vegetation and wildfire controls on sediment yield in bedrock landscapes, Geophysical Research Letters, 40, 1093–1097, https://doi.org/10.1002/grl.50277, 2013.

Earth Surface
Dynamics
Discussions

DiBiase, R. A., Lamb, M. P., Ganti, V., and Booth, A. M.: Slope, grain size, and roughness controls on dry sediment transport and storage on steep hillslopes, Journal of Geophysical Research – Earth Surface, 122, 941–960, doi:10.1002/2016JF003970, 2017.

Dippel, S., Batrouni, G. G., and Wolf, D. E.: How tranversal fluctuations affect the friction of a particle on a rough incline, Physical Review E, 56, 3645–3656, 1997.

5 Doane, T. H.: Theory and application of nonlocal hillslope sediment transport, PhD thesis, Vanderbilt University, Nashville, Tennessee, 2018.

Doane, T. H., Furbish, D. J., Roering, J. J., Schumer, R., and Morgan, D. J.: Nonlocal sediment transport on steep lateral moraines, eastern Sierra Nevada, California, USA, Journal of Geophysical Research – Earth Surface, 123, https://doi.org/10.1002/2017JF004325, 2018.

Doane, T. H., Roth, D. L., Roering, J. J., and Furbish, D. J.: Compression and decay of hillslope topographic variance in Fourier wavenumber domain, Journal of Geophysical Research – Earth Surface, 124, 60–79, doi: 10.1029/2018JF004724, 2019.

10 Dorren, L. K. A.: A review of rockfall mechanics and modelling approaches, Progress in Physical Geography, 27, 69–87, 2003.

Einstein, A.: Über die von der molekularkinetischen Theorie der Wärme geforderte Bewegung von in ruhenden Flüssigkeiten suspendierten Teilchen, Annalen der Physik, 17, 549–560, 1905.

Dominguez, H. and Zenit, R.: On the cooling law of a non-dilute granular gas, Revista Mexicana de Física, 53, 83–86, 2007.

Feller, W.: On the theory of stochastic processes, with particular reference to applications, Proceedings of the [First] Berke-
15 ley Symposium on Mathematical Statistics and Probability, 403–432, University of California Press, Berkeley, California, https://projecteuclid.org/euclid.bsmsp/1166219215, 1949.

Ferdowsi, B., Ortiz, C. P., and Jerolmack, D. J.: Glassy dynamics of landscape evolution, Proceedings of the National Academy of Sciences USA, 115, 4827–4832, 2018.

Forrester, S. F.: Boulder trundling, The Rucksack Club Journal, 1931.

20 Forterre, Y., and Pouliquen, O.: Flows of dense granular media, Annual Review of Fluid Mechanics, 40, 1–24, doi:10.1146/annurev.fluid.40.111406.102142, 2008.

Foufoula-Georgiou, E., Ganti, V., and Dietrich, W.: A nonlocal theory of sediment transport on hillslopes, Journal of Geophysical Research – Earth Surface, 755, 115(F2), https://doi.org/10.1029/2009JF001280, 2010.

Frey, P., and Church, M.: Bedload: a granular phenomenon, Earth Surface Processes and Landforms, 36, 58–69, doi: 10.1002/esp.2103, 2011.

25 Furbish, D. J.: Using the dynamically coupled behavior of land surface geometry and soil thickness in developing and testing hillslope evolution models, in: Prediction in Geomorphology, Geophysical Monograph Series, edited by: Wilcock P. and Iverson, R., 169–181, vol. 135, Washington, DC, 2003.

Furbish, D. J., and Doane, T. H.: Rarefied particle motions on hillslopes: 4. Philosophy, Earth Surface Dynamics, 2020c. (*in review*)

Furbish, D. J., Haff, P. K., Dietrich, W. E., and Heimsath, A. M.: Statistical description of slope-dependent soil transport and the diffusion-like
30 coefficient, Journal of Geophysical Research – Earth Surface, 114, F00A05, https://doi.org/10.1029/2009JF001267, 2009.

Furbish, D. J. and Haff, P. K.: From divots to swales: Hillslope sediment transport across divers length scales, Journal of Geophysical Research – Earth Surface, 115, F03001, doi: 10.1029/2009JF001576, 2010.

Furbish, D. J., Schmeeckle, M. W., and Roering, J. J.: Thermal and force-chain effects in an experimental, sloping granular shear flow, Earth Surface Processes and Landforms, 33, 2108–2117, 2008.

35 Furbish, D. J., Roseberry, J. C., and Schmeeckle, M. W.: A probabilistic description of the bed load sediment flux: 3. The particle velocity distribution and the diffusive flux, Journal of Geophysical Research – Earth Surface, 117, F03033, doi:10.1029/2012JF002355, 2012.

Furbish, D. J. and Roering, J. J.: Sediment disentrainment and the concept of local versus nonlocal transport on hillslopes, Journal of Geophysical Research – Earth Surface, 118, 1–16, doi: 10.1002/jgrf.20071, 2013.

Furbish, D. J., Roering, J. J., Almond, P., and Doane, T. H.: Soil particle transport and mixing near a hillslope crest: 1. Particle ages and residence times, Journal of Geophysical Research – Earth Surface, 123, https://doi.org/10.1029/2017JF004315, 2018a.

Furbish, D. J., Schumer, R., and Keen-Zebert, A.: The rarefied (non-continuum) conditions of tracer particle transport in soils, with implications for assessing the intensity and depth dependence of mixing from geochronology, Earth Surface Dynamics, 6, 1169–1202, https://doi.org/10.5194/esurf-6-1169-2018, 2018b.

Furbish, D. J., Williams, S. G., and Doane, T. H.: Rarefied particle motions on hillslopes: 3. Entropy, Earth Surface Dynamics, 2020b. (*in review*)

Furbish, D. J., Williams, S. G., Roth, D. L., Doane, T. H., and Roering, J. J.: Rarefied particle motions on hillslopes: 2. Analysis, Earth Surface Dynamics, 2020a. (*in review*)

Gabet, E. J.: Gopher bioturbation: Field evidence for non-linear hillslope diffusion, Earth Surface Processes and Landforms, 25, 1419–1428, 2000.

Gabet, E. J.: Sediment transport by dry ravel, Journal of Geophysical Research – Earth Surface, 108, 2049, doi:10.1029/2001JB001686, 2003.

Gabet, E. J., Reichman, O. J., and Seabloom, E. W.: The effects of bioturbation on soil processes and sediment transport, Annual Review of Earth and Planetary Sciences, 31, 249–273, 2003.

Gabet, E. J. and Mendoza, M. K.: Particle transport over rough hillslope surfaces by dry ravel: Experiments and simulations with implications for nonlocal sediment flux, Journal of Geophysical Research – Earth Surface, 117, F01019, doi:10.1029/2011JF002229, 2012.

Gerber, E. and Scheidegger, A. E.: On the dynamics of scree slopes, Rock Mechanics, 6, 25–38, 1974.

Gibbs, J. W.: Elementary Principles in Statistical Mechanics, Yale University Press, New Haven, Connecticut, 1902.

Haff, P. K.: Grain flow as a fluid-mechanical phenomenon, Journal of Fluid Mechanics, 134, 401–430, 1983.

Henann, D. L. and Kamrin, K.: A predictive, size-dependent continuum model for dense granular flows, Proceedings of the National Academy of Sciences, 110, 6730–6735.

Hosking, J. R. M. and Wallis, J. R.: Parameter and quartile estimation for the generalized Pareto distribution, Technometrics, 29, 339–349, 1987.

Houssais, M., Ortiz, C. P., Durian, D. J., and Jerolmack, D. J.: Onset of sediment transport is a continuous transition driven by fluid shear and granular creep, Nature Communications, 6, 6527, 2015.

Houssais, M. and Jerolmack, D. J.: Toward a unifying constitutive relation for sediment transport across environments, Geomorphology, 277, 251–264, https://doi.org/10.1016/j.geomorph.2016.03.026, 2017.

Hunt, M. L., Zenit, R., Campbell, C. S., and Brennen, C. E.: Revisiting the 1954 suspension experiments of R. A. Bagnold, Journal of Fluid Mechanics, 452, 1–24, 2002.

Ismail, K. A. and Stronge, W. J.: Impact of viscoplastic bodies: Dissipation and restitution, Journal of Applied Mechanics, 75, 061011, 2008.

Jaeger, H. M., Nagel, S. R., and Behringer, R. P.: Granular solids, liquids, and gases, Reviews of Modern Physics, 68, 1259–1273, 1996.

Jaynes, E. T.: Information theory and statistical mechanics, Physical Review, 106, 620–630, 1957a.

Jaynes, E. T.: Information theory and statistical mechanics. II, Physical Review, 108, 171–190, 1957b.

Jenkins, J. T. and Savage, S. B.: A theory for the rapid flow of identical, smooth, nearly elastic, spherical particles, Journal of Fluid Mechanics, 130, 187–202, 1983.

Jerolmack, D. J. and Daniels, K. E.: Viewing Earth's surface as a soft-matter landscape, Nature Reviews Physics, https://doi.org/10.1038/s42254-019-0111-x, 2019.

Kachuck, S. B. and Voth, G. A.: Simulations of granular gravitational collapse, Physical Review E, 88, 062202, doi: 10.1103/Phys-
RevE.88.062202, 2013.

Kirkby, M. J. and Statham, I.: Stone movement and scree formation, The Journal of Geology, 83, 349–362, 1975.

Kumaran, V.: Kinematic model for sheared granular flows in the high Knudsen number limit, Physical Review Letters, 95, 108001, 2005.

5   Kumaran, V: Granular flow of rough particles in the high-Knudsen-number limit, Journal of Fluid Mechanics, 561, 43–72, 2006.

Lamb, M. P., Scheingross, J. S., Amidon, W. H., Swanson, E., and Limaye, A.: A model for fire-induced sediment yield by dry ravel in steep
landscapes, Journal of Geophysical Research – Earth Surface, 116, F03006, doi: 10.1029/2010JF001878, 2011.

Lamb, M. P., Levina, M., DiBiase, R. A., and Fuller, B. M.: Sediment storage by vegetation in steep bedrock landscapes: The-
ory, experiments, and implications for postfire sediment yield, Journal of Geophysical Research: Earth Surface, 118, 1147–1160.
10   https://doi.org/10.1002/jgrf.20058, 2013.

Lee, D. B. and Jerolmack, D. J.: Determining the scales of collective entrainment in collision-driven bed load, Earth Surface Dynamics, 6,
1089–1099, 2018.

Luckman, B. H.: (2013) Processes, Transport, Deposition, and Landforms: Rockfall. In: John F. Shroder (ed.) Treatise on Geomorphology,
Volume 7, pp. 174–182, San Diego, Academic Press, 2013.

15   Moore, H. J., Hutton, R. E., Clow, G. D., and Spitzer, C. R.: Physical properties of the surface materials at the Viking landing sites on Mars,
US Geological Survey Professional Paper, https://doi.org/10.3133/pp1389, 1987.

Nakagawa, H. and Tsujimoto, T.: Sand bed instability due to bed load motion, Journal of Hydraulic Engineering, 106, 2023–2051, 1980.

Pähtz, T. and Durán, O.: The cessation threshold of nonsuspended sediment transport across aeolian and fluvial environments, Journal of
Geophysical Research – Earth Surface, 123, 1638–1666, doi: 10.1029/2017JF004580, 2018.

20   Pickands, J.: Statistical inference using extreme order statistics, The Annals of Statistics, 3, 119-131, 1975.

Quartier, L., Andreotti, B., Douady, S., and Daerr, A.: Dynamics of a grain on a sandpile model, Physical Review E, 62, 8299–8307, 2000.

Riguidel, F.-X., Hansen, A., and Bideau, D.: Gravity-driven motion of a particle on an inclined plane with controlled roughness, Europhysics
Letters, 28, 13–18, 1994a.

Risken H.: The Fokker–Planck Equation: Methods of Solution and Applications, Springer, Berlin, 1984.

25   Risso, D. and Cordero, P.: Dynamics of rarefied granular gases, Physical Review E, 65, 021304, 2002.

Roering, J. J.: Soil creep and convex-upward velocity profiles: theoretical and experimental investigation of disturbance-driven sediment
transport on hillslopes, Earth Surface Processes and Landforms, 29, 1597–1612, 2004.

Roering, J. J. and Gerber, M.: Fire and the evolution of steep, soil-mantled landscapes, Geology, 33, 349–352, doi:10.1130/G21260.1., 2005.

Roering, J. J., Kirchner, J. W., and Dietrich, W. E.: Evidence for nonlinear, diffusive sediment transport on hillslopes and implications for
30   landscape morphology, Water Resources Research, 35, 853–870, 1999.

Roering, J. J., Almond, P., Tonkin, P., and McKean, J.: Soil transport driven by biological processes over millenial time scales, Geology, 30,
1115–1118, 2002.

Roth, D. L., Doane, T. H., Roering, J. J., Furbish, D. J., and Zettler-Mann, A.: Particle motion on burned and vegetated hillslopes, Proceedings
of the National Academy of Sciences, www.pnas.org/cgi/doi/10.1073/pnas.1922495117, 2020.

35   Samson, L., Ippolito, I., Batrouni, G. G., and Lemaitre, J.: Diffusive properties of motion on a bumpy plane, European Physical Journal B, 3,
377–385, 1998.

Samson, L., Ippolito, I., Bideau, D., and Batrouni, G. G.: Motion of grains down a bumpy surface, Chaos, 9, 639–648, 1999.

Schumer, R., Baeumer, B., and Meerschaert, M. M.: Fractional advection-dispersion equations for modeling transport at the Earth surface, Journal of Geophysical Research – Earth Surface, 114, doi: 10.1029/2008JF001246, 2009.

Statham, I.: A scree slope rockfall model, Earth Surface Processes, 1, 43–62, 1976.

Stronge, W. J.: Rigid body collisions with friction, Proceedings of the Royal Society of London A, 431, 169–181, 1990.

Stronge, W. J.: Impact Mechanics, Cambridge University Press, Cambridge, 2000.

5 Tesson, P. -A., Conway, S. J., Mangold, N., Ciazela, J., Lewis, S. R., and Mège, D.: Evidence for thermal-stress-induced rockfalls on Mars impact crater slopes, Icarus, 342, 113503, https://doi.org/10.1016/j.icarus.2019.113503, 2020.

Tsujimoto, T.: Probabilistic model of the process of bed load transport and its application to mobile-bed problems, PhD thesis, Kyoto University, Kyoto, Japan, 1978.

Tajima, H. and Fujisawa, F.: Projectile trajectory of penguin's faeces and rectal pressure revisited, arXiv:2007.00926 [physics.bio-ph], 2020.

10 Tucker, G. E. and Bradley, D. N.: Trouble with diffusion: Reassessing hillslope erosion laws with a particle-based model, Journal of Geophysical Research – Earth Surface, 115, F00A10, doi: 10.1029/2009JF001264, 2010.

Volfson, D., Meerson, B., and Tsimring, L. S.: Thermal collapse of a granular gas under gravity, Physical Review E, 73, doi: 10.1103/PhysRevE.73.061305, 2006.

van Zon, J. S., and MacKintosh, F. C.: Velocity distributions in dissipative granular gases, Physical Review Letters, 93, 038001, doi: 15 10.1103/PhysRevLett.93.038001, 2004.

von Smoluchowski M.: Zur kinetischen Theorie der Brownschen Molekularbewegung und der Suspensionen, Annalen der Physik, 326, 1685 756–780, 1906.

Yu, P., Schröter, M., and Sperl, M.: Velocity distribution of a homogeneously cooling granular gas, Physical Review Letters, 124, 208007, doi: 10.1103/PhysRevLett.124.208007, 2020.